Reconstruction of the Late Miocene to Pliocene continental succession of Samos Island: Palaeoenvironmental implications for the Eastern Aegean domain

Youri Hamon, Rémy Deschamps, Christian Gorini, Dimitris Sakellariou, Cédric Bailly, Tarik Kernif, Alina Bérénice Christ, Mathilde Adelinet, Jerome Fortin

Hamon Youri (Orcid ID: 0000-0003-4794-0254)
Deschamps Remy (Orcid ID: 0000-0002-0888-3456)

Reconstruction of the Late Miocene to Pliocene continental succession of Samos Island: Palaeoenvironmental implications for the Eastern Aegean domain

Running head – Palaeoenvironments in the Eastern Aegean domain

HAMON Youri [(1;*)]; DESCHAMPS Rémy [(1)]; GORINI Christian [(2)]; SAKELLARIOU Dimitris [(3)]; BAILLY Cédric [(4)]; KERNIF Tarik [(5)]; CHRIST Alina Bérénice [(1)], ADELINET Mathilde [(6)]; FORTIN Jérôme [(7)]

[(1)] Earth Sciences and Environmental Technologies Division, IFP Energies nouvelles, 1 et 4 avenue de Bois-Préau, 92852 Rueil-Malmaison, France

[(2)] Sorbonne Université, UMR 7193 CNRS-UPMC, Institut des Sciences de la Terre Paris, F-75005 Paris, France

[(3)] Institute of Oceanography, Hellenic Center for Marine Research, 19013 Anavyssos, Greece

[(4)] Université Paris-Saclay, CNRS, GEOPS, 91045, Orsay, France

[(5)] Université Rennes 1, Géosciences Rennes UMR CNRS 6118, 35000, Rennes, France

This article has been accepted for publication and undergone full peer review but has not been through the copyediting, typesetting, pagination and proofreading process which may lead to differences between this version and the Version of Record. Please cite this article as doi: 10.1002/dep2.249

(6) IFP Energies nouvelles, IFP School, 1 et 4 Avenue de Bois-Préau, Rueil-Malmaison Cedex, France

(7) Laboratoire de Géologie, Ecole normale supérieure/CNRS UMR8538, PSL Research University, Paris, France

* Corresponding author: Youri Hamon; youri.hamon@ifpen.fr

Abstract – On the Island of Samos (East Aegean region, Greece), two sedimentary basins are filled by thick continental series dated to the Late Miocene to Early Pliocene. A multi-disciplinary study has been performed including 1) the definition of 21 sedimentary facies, 2) a review of the biological components and 3) carbon, oxygen and strontium stable isotope analyses. The succession is characterised by various depositional settings and hydrochemical compositions. Five main stages of basin evolution have been identified: 1) The Late Serravalian is marked by the development of alluvial fans and fan delta; 2) during the Lower Tortonian, isolated shallow lakes with variable salinity, from fresh to brackish, developed under warm and relatively humid conditions; 3) the Middle to Upper Tortonian is marked by the development of a large and deep lake with saline and alkaline waters, under colder and drier conditions; 4) the Latest Tortonian to Messinian period is represented by an ephemeral alluvial system, developed under a dry climate; 5) during the Zanclean, a palustrine and paludal wetland system, dominated by tufa carbonates, developed under moderately humid conditions. This succession is of particular interest for the reconstruction of the palaeoenvironmental evolution of the transition zone between the Mediterranean domain, and the Paratethys and circum-Paratethys areas. The geochemical data and the presence of flora (diatoms) and fauna (gastropods) of marine affinity suggest transient ingressions of marine-related water or groundwater inflows as early as the Lower Tortonian. The Samos succession records the complex interaction between the regional geodynamics and climate. The extensional regime of the Eastern Aegean zone generates subsidence, interrupted in the mid-Tortonian (9 Ma) by a brief compressive event and a major

exposure of the basins. Furthermore, the Late Miocene progressive aridification, followed by a change to a more humid climate (Pliocene) is also a major driver of the sedimentation.

Keywords - Depositional models, East-Aegean area, lacustrine carbonates, Late Miocene, palaeoclimate, tectonic.

1. Introduction

Lacustrine sedimentary systems record the complex interaction of numerous parameters: 1) physiography (vegetation, alteration and erosion); 2) environments (temperature, precipitation, volcanic events…); 3) sedimentary processes (biotic and abiotic); and 4) active tectonics (stress rotations, faulting or flexuring, subsidence…). Lakes are particularly sensitive to climate changes and lacustrine sediments are accurate and precise indicators of environmental changes (Platt & Wright, 1991; Alonso-Zarza et al., 2012). Therefore, they constitute some of the most complete and best-preserved archives of past environmental conditions (Dean & Fouch, 1983; Platt & Wright, 1991; Gierlowski-Kordesch, 2010).

As such, the Late Miocene-Pliocene continental succession of Samos Island (Eastern Aegean Sea) is of particular interest (Hamon et al., 2017). It developed in the Aegean/Anatolian region, in an active tectonic setting associated with the back-arc deformation of the Africa-Europe subduction zone (Le Pichon & Angelier, 1981; Jolivet et al., 1994). Due to their key position at the transition between two geodynamic blocks (East Aegean and Anatolian), the Samos basins are of particular interest when attempting a reconstruction of the long-debated regional geodynamics and palaeogeography (Le Pichon & Angelier, 1981;

Jolivet et al., 1994; Taymaz et al., 2007; Brun et al., 2016; among many others). Additionally, these series were deposited during a period of important climate perturbations (Eronen et al., 2009; Palcu et al., 2019; Butiseacă et al., 2021) and a major environmental crisis, the so-called Messinian Salinity Crisis (MSC; Roveri et al., 2014; Flecker et al., 2015). Depending on the palaeogeographic location (Mediterranean Sea versus Paratethys and circum-Paratethys), these climate perturbations are not synchronous and do not have the same expression. Being located between these two palaeogeographic entities, the Samos basins are a perfect case study to unravel the effect of such climatic forcing on the development of lacustrine carbonate systems.

Based on an extensive multidisciplinary database, including sedimentological and geochemical (strontium, carbon and oxygen stable isotopes) analyses, associated with a thorough review of previously published palaeontological material (molluscs, diatoms and pollen), the present article brings new insights on the evolution of East-Aegean, Miocene continental depositional systems. The sedimentary record of the Samos basins is then compared to the ones of neighbouring basins, which will provide new constraints on the Neogene palaeogeographic, palaeoclimatic and geodynamic context of the Eastern Aegean region.

2. Geological setting

The Island of Samos (Figure 1) has been the subject of numerous papers, on different topics. Samos is famous for its unique Late Miocene fossiliferous sites of mammal fauna (Koufos et al., 1997; Koufos, 2006; Giaourtsakis & Koufos, 2009; Kostopoulos, 2009a, 2009b; Koufos et al., 2011). From a geodynamic point of view, it also occupies a key position in the back-arc Africa-Europe subduction zone, at the transition between two domains, the Aegean region and the western Anatolia extensional province (Ring et al., 1999; Ring et al., 2007; Jolivet et al., 2013; Roche et al., 2019).

The Samos basement mainly consists of a succession of four stacked tectono-metamorphic units, the Selcuk, Ampelos, Agios Nikolaos and Kerketas nappes, made up of metamorphic (marble, quartzite, schists of Carboniferous to Cretaceous age) or sedimentary rocks (dolostone) (Ring et al., 1999; Löwen et al., 2015). A last non-metamorphosed unit, the Kallithea nappe is made of sandstones, serpentinised peridotite lenses, spilite and diabase with red radiolarites (Theodoropoulos, 1979) and was locally intruded at *ca* 10 Ma by igneous dykes (Mezger et al., 1985; Pe-Piper & Piper, 2007). These nappes are the remains of the crustal-scale orogenic wedge derived from the subduction of African continental blocks below Eurasia (Ring et al., 1999; Roche et al., 2019).

Since the Early Oligocene, the region has been mainly affected by back-arc extension, driven by the progressive southward retreat of the African slab (van Hinsbergen & Schmid, 2012; Brun et al., 2016). During the middle Miocene, a slab tear occurred below Western Anatolia, with a faster retreat of the western part of the slab. This generated a differential extension between the Aegean and Anatolian domains, with a greater extension westward of the tear, compared to the Anatolian block (Jolivet et al., 2013). In Samos, this extension induces the formation of two sedimentary basins, filled by alluvial and lacustrine sediments; the Karlovassi Basin (West Samos), filled with a 600 m thick sedimentary succession and the Mytilini Basin (East Samos) which displays a 1,200 m thick succession (Figure 1; Theodoropoulos, 1979; Weidmann et al., 1984; Stamatakis et al., 2009).

2.1. Mytilini Basin

In the Mytilini Basin (eastern basin; Figure 1), Weidmann et al. (1984), following Meissner (1976), described five lithostratigraphic formations deposited unconformably on the metamorphic basement (Figure 2). Radiochronological dating on volcanic rocks, magnetostratigraphy and mammal ages provide precise age constraints for this sedimentary infill (Ioakim & Solounias, 1985; Sen & Valet, 1986; Kostopoulos et al., 2003; Pe-Piper & Piper, 2007, Koufos et al., 2011).

At the base, two formations occur; the Basal Conglomerate, made of conglomerates with locally derived pebbles of basement, interbedded with claystones, followed by the palustrine and lacustrine marls and marly limestones of the Pythagorion Formation (Figure 2). The Basal Conglomerate and the Pythagorion formations are dated from 12 Ma to 10.8 Ma. The Hora Formation (from 10.8 to 8.6 Ma) is mainly composed of lacustrine limestones and diatomaceous silts (Owen et al., 2011). In this article, for the sake of clarity, the Hora Formation is informally subdivided into four units - Figures 2 and 3). The first unit (U1) is composed of well-stratified dolostones and limestones, often affected by slump structures in the upper part. The second unit (U2) is characterised by alternating well-stratified limestones and diatomite layers. The third unit (U3) consists of a thick package of diatomite-dominated facies. The last unit (U4) is dominated by a variety of well-stratified shallow limestone facies. The Hora Formation is topped by a regional unconformity, associated with an angular difference between 8 to 15° depending on the outcrops.

Overlying the Hora Formation, the Mytilini Formation is composed of alluvial terrigenous (conglomerates, sandstones and claystones) and volcaniclastic sediments, deposited during the late Tortonian and Messinian periods. Weidmann et al. (1984) subdivided the Mytilini Formation into five units (Figures 2 and 4): 1) the Old Mill Beds; 2) the Gravel Beds; 3) the White Beds; 4) the Main Bone Beds; 5) the Marker Tuffs. Finally, the transition with the Kokkarion Formation, was dated at 5.7 Ma by magnetostratigraphy (Sen & Valet, 1986), which is in agreement with the K/Ar ages of Weidmann et al. (1984). This last formation is made of palustrine and paludal carbonates and is attributed to the Early Pliocene (Zanclean).

2.2. Karlovassi Basin

A coeval succession is observed in the Karlovassi Basin, with slight differences (Kantiranis et al., 2007; Stamatakis et al., 2009). The Basal Conglomerate and an equivalent of the Pythagorion Formation are observed and respectively composed of conglomerates interbedded with claystones, and lacustrine silty carbonates interbedded with thick intervals of volcanic tuffs and tuffaceous clays and marls (Figure 2).

In the southern part of the basin (Marathokampos, this study), the Hora equivalent formation is composed of well stratified, thinly laminated limestones, with a few occurrences of decimetre-scale tuff layers. No diatomite facies were observed within this section (Figure 2). In the central and northern part of the basin, this formation is mainly composed of dolomitic marlstones and tuffs, associated with scattered evaporitic minerals, like gypsum, colemanite and celestite forming nodules, lenses, or fissure fillings (Helvaci et al., 1993; Stamatakis et al., 2009). As in the Mytilini Basin, the Hora equivalent formation is affected at its top by an unconformity with angular differences of between 8 to 15° (Kantiranis et al., 2007).

Overlying this unit is a terrigenous succession that may represent an equivalent of the Mytilini Formation. It is particularly rich in volcanic tuff layers and shows fewer occurrences of conglomerate facies when compared to deposits in the Mytilini Basin (Figure 2). Finally, Pliocene freshwater paludal carbonates similar to the Kokkarion Formation are observed at the top of the succession (Theodoropoulos 1979, Stamatakis & Economou, 1991).

3. Methods

3.1. Field descriptions and petrography

The available outcrops in Samos Island prevents the description of a continuous stratigraphic section of the whole basin infill. However, several outcrops, located both in the Eastern Mytilini and Western Karlovassi basins, were studied and correlated to provide a set of 11 main sections (Figure 1). They were completed by secondary observations (mapping, logging of minor sedimentary sections; Figure 1) to give a synthetic overview of the sedimentary succession. The 11 main sections were described in detail (Figures 3 and 4) and sampled to analyse the facies composition and fabric. The carbonate facies were described following the revised Dunham classification formulated by Lokier and Al Junaibi (2016).

Petrographic analyses were conducted on 169 thin sections, distributed across all sections. They were stained with alizarin red-S and potassium ferricyanide to highlight the distribution of the main carbonate minerals (Dickson, 1966). Petrographic observations were carried out with a Nikon Eclipse LV100 POL microscope.

To complete the petrographic work, a synthesis of previously published palaeontological data has been compiled. These involve spores and pollen (Ioakim & Solounias, 1985; Ioakim et al., 2005; Ioakim & Koufos, 2009; Koufos et al., 2011), diatoms (Owen et al., 2011) and gastropods (Koufos et al., 2011; Owen et al., 2011; completed by observations reported on here).

3.2. Carbon and oxygen isotopes

A total of 139 rock samples were drilled and analysed for oxygen (O) and carbon (C) isotope analysis (Supplementary Material Table S1). The phases preferentially extracted were homogeneous micrite and dolomicrite. Analyses have been made at the Friedrich-Alexander University of Erlangen-Nürnberg,

which provided the following specific procedure and specifications: the carbonate powders were reacted with 100% phosphoric acid at 70°C using a Gasbench II connected to a ThermoFinnigan Five Plus mass spectrometer. All values are reported in per mil relative to V-PDB (Vienna Pee Dee Belemnite) by assigning a $\delta^{13}C$ value of +1.95‰ and a $\delta^{18}O$ value of -2.20‰ to the NBS19 standard. Reproducibility was checked by replicate analysis of laboratory standards and is better than ± 0.08. By default, Oxygen isotope values of dolomite were corrected using the oxygen fractionation factors between the $\delta^{18}O$ of the carbonate and that of the acid-extracted CO_2 at 100°C (1.00913) provided by Rosenbaum and Sheppard (1986).

3.3. Strontium isotopes

A set of 27 carbonate powder samples were selected from the initial sample set and analysed for $^{87}Sr/^{86}Sr$ ratios at the Scottish Universities Environmental Research Centre laboratory (Supplementary Material Table S1), which provided the following specific procedure and specifications. Strontium isotope analyses were performed on 1 mg of powder in 2.5 M HCl. The separation between the two components was done by ionic exchange. Samples were loaded on two single Re filaments and run on a VG Sector 54e thermal ionisation mass spectrometer. The $^{87}Sr/^{86}Sr$ ratios were then normalised to a ratio value of $^{87}Sr/^{86}Sr$ = 0.1194. The precision was better than ±0.04 ‰.

4. Facies analysis

The Miocene succession of Samos Island is characterised by a mixing of terrigenous (T), carbonate (C) and volcaniclastic (V) deposits, characteristic of alluvial plain, fluvial and lacustrine depositional environments. The facies analysis enables the definition of 21 facies, presented in Table 1. These facies were grouped in seven facies associations, defined, and then attributed to a specific depositional environment based on their elementary constituent facies, vertical stacking, lateral facies change and overall geometry.

4.1. FA1: Fan-derived alluvial facies association

This facies association is dominantly made up of erosively-based, normally graded, poorly sorted, matrix-supported, structureless conglomerates (Facies T1; Figures 5A,B,C), organised into metres-thick, fining upwards beds. They are capped by decimetre to metre-thick laterally continuous reddish silty claystone containing whitish carbonate nodules, frequent root traces and desiccation cracks (Facies T5, Figure 5H,I). Channelised clast-supported polygenic conglomerates with coarse-grained sandstone matrix are locally observed, with a basal erosional surface truncating the underlying deposits (Facies T2; Figure 5D,E). This facies is often associated with coarse to medium-grained sandstones with floating pebbles showing 3D cross-stratifications passing upwards to plane parallel laminations (Facies T3; Figure 5E,F), organised into metre(s)-thick, fining-upwards beds.

This facies association is interpreted as being deposited in a fan-derived alluvial environment: the dominant facies (i.e., Facies T1) shows laterally persistent bedding, a matrix-rich nature and a lack of traction-produced sedimentary structures that suggest deposition by mass-flows, associated with high-density gravity flash-discharge events (Sohn et al., 1999). The uppermost sandy part of the facies may suggest more diluted flows occurring during the following waning stage (Chanvry et al.; 2018). The reddish silty claystones (Facies T5) are interbedded with the previous facies, and were deposited in a continental,

alluvial plain environment. Reddish clayey to silty material, root traces and carbonate concretions are typical of floodplain deposits affected by pedogenesis (Reineck & Singh, 1980; Miall, 1996). These facies are generally interpreted as the distal reaches of alluvial fans (Nemec & Steel, 1984), or as the proximal part of braidplain megafans (Leier et al., 2005; Schmitz & Pujalte, 2007). In these environments, the influence of fluvial streams is evidenced by the clast-supported fabric and clast imbrication, the presence of trough-cross bedding and the erosive base which suggest that both T2 conglomerates and T3 coarse-grained sandstones were deposited by traction processes, possibly the migration of large, gravelly, transverse bars (Smith, 1990; Miall, 1996; Boulton et al., 2019). Williams and Rust (1969), Bridge (1993) or Chanvry et al. (2018) interpreted such facies as deposited in a braided channel network associated with high discharge flooding events.

4.2. FA2: Stream-derived alluvial facies association

This facies association is exclusively composed of terrigenous facies. It mainly consists of coarse to medium-grained, moderately sorted sandstones with floating pebbles, showing a fining upward trend, a lower erosive surface and an upper planar one, often affected by root traces and rootlets (facies T3; Figure 5E,F). This facies is locally associated with metre(s)-thick, fining upward beds marked by a distinct erosional basal surface (Facies T2), which truncates the underlying deposits and usually defines low-relief, channelised morphologies (5-10 m wide, for 1-2 m thick; Figure 5D). Clasts are poorly sorted, subangular to angular, of basement nature and often show some imbrication. Plant debris is abundant, but no fauna was observed. This facies often exhibits badly expressed trough-cross bedding. Facies T2 and T3 are often associated with discontinuous lenticular beds, a few decimetres thick, with a non-erosional,

undulatory base (Facies T4; Figure 5G). Facies T4 is typically medium to fine-grained, poorly to moderately sorted and shows a planar horizontal lamination. Local granule lenses are occasionally observed on bedding planes.

This facies association also locally includes metre-scale, laterally continuous massive beds (Facies V1; Figure 6A), with a well-defined, regular planar bedding, and sharp, but non-erosive basal contact, and no internal truncation surfaces (Figure 6A,B). This facies is dominantly composed of fine-grained vitreous fragments composing the matrix, with only very minor plagioclase and pyroxene crystals. The lithic fraction may be absent in some layers. This facies lacks any sedimentary structures, apart from rare root traces affecting the top of a few beds. This facies generally alternates with reddish silty claystone (facies T5; Figure 6A).

This stream-derived alluvial facies association is interpreted as braided fluvial channel fill, made up of the depositional products of subaqueous migrating transverse and longitudinal bars (Horton & Schmitt, 1996; Miall, 1996) infilling previous eroded channel conduits. Root networks on the upper surface of beds suggest the development of palaeosoils, occurring during low water levels and channel abandonment (Smith et al., 1989; Miall, 1996). The intercalation of pyroclastic material (Facies V1), despite the absence of typical fluvial sedimentary structures and the sharp compositional and textural contrast with the underlying non-volcanic deposits, suggest a subaerial mode of deposition, like pyroclastic fallout deposits, originating from subaerial eruption columns (Cole & DeCelles, 1991; Pe-Piper & Piper, 2007). The alternation with facies T5 and occurrences of root traces may also indicate a subaerial floodplain environment.

4.3. FA3: Marginal palustrine facies association

This facies association is mainly composed of three facies. Blue green marls (facies C1) form decimetre to metres-thick layers, with a massive aspect, and a faint planar lamination (Figure 7A). This facies consists of silt-size (40-60 µm) subangular quartz grains and micas in a marly matrix. It is particularly rich in plant debris, and locally, some darker intervals rich in organic matter and pyrite are observed. A few entire gastropods are present. Facies C2 is abundant and organised into decimetre to metre-thick beds that are tabular and laterally continuous. This facies contains entire and broken gastropods (Figure 7C and E) and Characean gyronites, while plant stems and leaves are common. Facies C3 is less abundant and occurs as occasional decimetre(s)-thick tabular beds. These packstones are dominated by very uniform (in shape and size) peloids, but also show gastropod debris, disarticulated valves of ostracods and rare Characean gyrogonites (Figure 7F). Rounded clay clasts are frequent. These three facies are often bioturbated and always affected by vertical root traces (Figure 7D), elongated whitish root concretions and nodular whitish carbonate glaebules (Figure 7B).

The fine-grained nature of facies C1 and C2 suggests a low-energy environment dominated by decantation processes, while the abundance of detrital material suggests a proximal environment, with detrital influx (Freytet, 1973; Lettéron et al., 2018). The local presence of organic matter (plant debris, pyrite...) may denote restricted conditions and episodic periods of dysoxic conditions (Camoin et al., 1997). These facies represent a shallow, quiet and restricted environment, associated with inner marginal conditions (Castle, 1991; Alonzo-Zarza, 2003). As suggested by their uniform shape and size, the peloids of facies C3 may be of faecal origin, produced by crustaceans, worms or gastropods (Freytet & Verrechia, 2002). The packstone texture may be due to a dense population of such pellet-producing organisms rather than high-energy conditions (Finkelstein et al., 1999; Lettéron et al., 2018). This is in line with the important bioturbation and the presence of gastropods and ostracods observed in C3, as well as the absence of erosional features or sedimentary structures. Such features indicate a shallow, littoral lacustrine environment (Letteron et al., 2017; Bailly et al., 2019).

Finally, root traces and cavities, glaebules and root concretions are indicative of pedogenesis during episodic exposure (Klappa, 1980), which is consistent with the presence of desiccation cracks and fenestrae. Their systematic occurrence in the three facies of this facies association indicates repeated alternating periods of exposure and shallow subaquatic conditions, typical of a palustrine to littoral setting (Armenteros et al., 1997; Freytet & Verrechia, 2002; Alonzo-Zarza, 2003; Gierlowski-Kordesch, 2010; Armenteros & Edwards, 2012).

4.4. FA4: Lacustrine sublittoral facies association

This facies association is dominated by facies C5a, a well-stratified mudstone organised in thinly bedded, decimetre(s)-thick, yellowish to greyish, tabular layers, with non-erosional flat top and bottom surfaces (Figure 7I). This facies is composed of a micritic matrix, with only a few peloids, gastropods and micritic intraclasts (less than 5 %). The faint planar lamination observed macroscopically is marked in thin section by sub-millimetre laminae richer in clay and pyrite, alternating with more micritic laminae (Figure 7J). Two subordinate facies, C4 and V2, are also observed in FA4, occurring as isolated beds interstratified with facies C5. Facies C4 is organised into decimetres-thick tabular, slightly erosive beds, that often show some planar to cross-bedded laminations or wave ripples (Figure 7G). In rare cases, some flat hummocky cross-stratification (HCS)-like structures occur. This well-sorted grainstone is dominated by irregular micritic peloids (no visible internal structure), associated with some micritised ooids, rounded micritic intraclasts and small quantities of gastropod debris and fish remains (Figure 7H). Facies V2 occurs at several stratigraphic levels in the studied succession, with various thickness (Figure 6C,D). The most pronounced occurrence is situated in the Kavouraki / Mavratzei area (Figure 3) with a 40 to 50 m thick, light grey massive layer, lying on a 10 m thick sheet of basalt. Other thinner occurrences form decimetre to metre-thick beds, interstratified with facies C5a and C5b, throughout the Hora Formation. They show an overall fining

upward trend from very coarse to medium-grained, poorly sorted material, made of subhedral to euhedral phenocrysts of plagioclase and pyroxene embedded in a matrix of silt-size unidentified vitreous fragments (Figure 6F). A minor fraction of lithic fragments composed of clasts of basalts and carbonates is also present. Some convolute structures occur at several levels within the layer (Figure 6E).

The mudstone texture and the fine-grained nature of facies C5a suggest a quiet environment dominated by decantation processes, without any hydrodynamism (Zhang et al., 1998). Laminae preservation suggests deposition within an environment without bioturbation, pedogenesis or any other process capable of destroying primary sedimentary structures. These criteria are typical of a low-energy offshore domain, associated with a sublittoral lacustrine environment (Freytet & Verrechia, 2002; Keighley, 2008). The texture (well-sorted, grain-supported) and sedimentary structures (cross-bedding, HCS) of facies C4 indicate episodic high-energy conditions such as those produced by storms and currents driven by fluctuating winds (Clausing, 1990; Arp, 1995; Ainsworth et al., 2012). Finally, facies V2 has been interpreted as felsic pyroclastic tuff layers (Pe-Piper & Piper, 2007). The high matrix content, poor sorting, the lack of stratification, or flow structures suggest a dominant mass flow mode of deposition (Smith, 1986). The fining upward trends may also indicate a decrease of energy, and a probable decantation of the finest particles (ashes, not necessarily preserved) occurring after the event. The lithic fraction may indicate mixing with water and entrainment of substrate sediments as pyroclastic flows transformed into pyroclastic debris flows (Cole & DeCelles, 1991). The intercalations of lacustrine facies (and even scarce faunal remains) in the upper part of the tuff layers, suggests a subsequent preservation under low-energy conditions in a sublittoral lacustrine environment, which is in line with previous interpretations of Weidmann et al. (1984).

4.5. FA5: Marginal evaporative facies association

This facies association is composed of three dolomitic facies. Facies C6 and C7 consist of decimetre-thick irregular beds, with a dark grey colour (Figure 8A), lacking any faunal remains. Facies C6 shows lenticular-tabular lenses (from 0.1 to 2 mm length) originally filled by gypsum, now mostly dissolved (Figure 8A,B). Some larger spherical voids (0.2 - 1 cm) occur and may correspond to solution-enlarged lenses or to dissolution cavities of nodular gypsum, now dissolved. Facies C7 is made up of a planar-laminated bindstone. Sub-horizontal, wavy, micrite laminae (100 µm to 1 mm thick) alternates with dolomicrosparite laminae (up to 0.5 mm thick). Occasionally, some peloid-rich laminae are also observed. The top of the laminated dolomudstone beds show some brecciation, forming a centimetres-thick layer, made of poorly sorted, millimetre to centimetre sized, subangular clasts consisting of reworked chips. Finally, Facies C8 consists of decimetre(s) -thick, whitish, well-stratified tabular beds, with flat top and bottom surfaces. They form metre-thick intervals that alternate with the two previous dolomitic facies (Figure 8C). They are composed of dolomudstone, mostly azoic (rare *Hydrobia* gastropod occurrences), lacking any sedimentary structure. Owen et al. (2011) described the rare occurrence of corroded diatoms (*Cyclotella aegaea*) in a few beds. Facies C8 may contain in variable proportions dark-brown isolated chert nodules, aligned parallel to bedding, and in some cases tabular flint layers.

Facies C6 and C7 are commonly reported from shallow lacustrine settings (Talbot & Allen, 1996; Wattine et al., 2003, 2017; Lettéron et al., 2017, 2018). In facies C6, the layered organisation, the horizontal alignment of gypsum crystals and their well-developed lenticular habit suggest synsedimentary subaqueous formation in a hypersaline shallow lake margin, under evaporitic conditions (Mees et al., 2012; Bustillo et al., 2017). Its association with facies C7 supports this interpretation. The occurrence of planar fenestrae and brecciation at the top of beds suggests episodic exposure; the small-scale undulations and the alternation of micritic and microsparitic laminae suggest microbial laminae, also associated with very shallow lake margins (Lettéron et al., 2017; Roche et al., 2018). As well as the two previous facies, facies C8 has been associated with a shallow, littoral setting. The muddy texture suggests low-energy conditions,

possibly associated with a mudflat environment (Bustillo et al., 2002, 2017; Lettéron et al., 2017). The absence of exposure criteria indicates permanently submerged conditions, in a more distal and slightly deeper environment than the two previous dolomitic facies.

4.6. FA6: Lacustrine profundal facies association

This facies association is mainly made up of three facies: facies C5a (described previously), facies C5b, well-stratified limestones with syn-sedimentary deformation features and facies C9, thinly laminated papyraceous diatomites. Facies C5b is observed in Units 1 and 2 of the Hora Formation. It shows similar characteristics to facies C5a, but also exhibits metre-scale slumping (Figure 7K), overturned-beds, creeping balls, as well as metre-scale disharmonic folds that are draped and overlain by planar conformable beds (Figure 7L). Decimetre-thick convolute structures are also observed. These deformation structures may also be associated with brecciated layers. Facies C9 forms decimetre(s)-thick intervals alternating with facies C5a and C5b (Figure 3). It displays a progressive thickening upward along the Hora Formation, reaching tens of metres in Unit 3. This facies was studied in detail by Owen et al. (2011). It consists of three types of alternating millimetre to centimetre-thick laminae (Figure 8D,E): 1) carbonate micritic laminae; 2) diatomite laminae, often recrystallised and cemented by a silica cement and; 3) diatomaceous silt (Zahajská et al., 2020). These laminae are often deformed, showing a crenulated aspect, folded (small-scale slumps) and even brecciated, forming discontinuous flat imbricated pebbles of diatomite overlain by later sediments.

The slumps, folds and convolute features observed in facies C5b suggest synsedimentary plastic deformation of a partially lithified sediment and imply the presence of a depositional slope, associated with the sublittoral to profundal lacustrine domain (Rodriguez-Pascua et al., 2000; Keighley, 2008). Weidmann et al. (1984) and Owen et al. (2011) interpreted these features as indicative of a potential seismicity that triggered the deformation. An alternative explanation

could be related to the high sedimentation rate occurring during the Hora Formation, that caused loading and triggered instability and initiated sliding on the slope (Rodriguez-Pascua et al., 2000).

Diatoms are common in lakes since the Miocene and may be found in several sub-environments, from littoral to profundal (Gierlowski-Kordesch, 2010; Hofmann et al., 2020). However, laminated diatomites, also described as varved lacustrine diatomites are associated with profundal lacustrine settings (Owen & Crossley, 1992; Lindqvist & Lee, 2009; Sasaki et al., 2020). The well-preserved lamination, their high lateral continuity and consistent thickness, the absence of exposure criteria and the association with facies C5a and C5b also suggest deposition in low-energy, deep environment (Lindqvist & Lee, 2009; Gierlowski-Kordesch, 2010). The diatom floras are of low diversity, but seem to indicate alkaline and saline conditions, possibly evolving through time (Owen et al., 2011; also see part 5.2 of the present work).

4.7. FA7: Paludal tufa facies association

This facies association was only observed in the Kokkarion Formation. It is composed of four facies (C10 to C13), generally organised in metre(s)-thick sets of beds, separated by blue-green marls (facies C1, previously described).

Facies C10 is composed dominantly of peloids and intraclasts with various sizes and shapes (Figure 8F), poorly sorted, embedded in a dark micritic matrix. Locally, some charophyte gyrogonites are present, as well as phytoclasts, gastropods and rare silt-sized quartz (Figure 8G). The facies is affected by numerous root moulds and circum-granular cracks, usually developing around oversized clasts (Figure 8H). Pseudomicrokarstification (sensu Freytet & Verrecchia, 2002)

is also observed below irregular surfaces, with decimetre-size enlarged root hollows, infilled by coarse intraclasts and microsparitic silt. Facies C11 and C12 are stratigraphically and laterally closely associated. At outcrop, facies C11 (phytoherm framestone) occurs as laterally discontinuous metre-scale patches and beds with irregular boundaries. They show a dense intricate amalgamation of millimetre- to centimetre-scale stem moulds, in life position, developed around macrophytes, most probably phragmites (Figure 8J). These moulds exhibit a laminated microstructure with alternating calcite micrite and spar to microspar laminae (Figure 8K) and are embedded in a dark beige micritic to peloidal matrix. Facies C12 shows decimetres-thick beds with irregular bedding planes and root traces at their top. It consists of a rudstone made of broken stem-moulds, several millimetres to centimetres in diameter and of variable length (centimetre to decimetres), with no particular organisation or orientation (Figure 8I). Both C11 and C12 contain gastropods, charophyte thalli and gyrogonites, and rare oncoids. Finally, facies C13 is organised in decimetre to metre-thick massive beds, showing a fining-upward trend and an erosive, channelised base. It consists of a floatstone facies with scattered dark beige millimetre to centimetre rounded micritic oncoids, millimetre-sized phytoclasts, intraclasts embedded in a dark beige matrix, occasionally microporous (Figure 8L). Fragments of gastropods have been observed in a few samples.

The lacustrine biota and charophytes observed in these facies suggest primary deposition in a shallow environment, between 0 to 4 m depth (Asaeda et al., 2007). In the case of facies C10, however, the primary facies is extensively affected by root moulds, circum-granular cracks or pseudomicrokarstification that point towards exposure and pedogenesis associated with the palustrine domain (Klappa, 1980; Freytet & Verrecchia, 2002). The peculiar fabric of this facies is similar to the intraclastic limestones described by Alonso-Zarza (2003) and considered to be the most widespread facies of the palustrine domain. Following Pedley (1990, 2009), facies C11, C12 and C13 are typical of a paludal tufa-dominated system: facies C11 (phytoherms) may be interpreted as the remains of anchored frameworks of hydrophytal and semi-aquatic macrophytes, frequently colonised by a dense micro-film of cyanobacteria. For Arenas et al. (2007), this facies represents the development of plants typical of poorly drained, humid areas, in which their submerged parts were coated by calcite. Considering

the height of the phytoherms as a measure of the water depth (Riding, 1979), the latter probably does not exceed 2 m. Phytoclast rudstones (C12) are frequent in many fluvial and fluvio-lacustrine tufa systems (Ordóñez & García del Cura, 1983; Ford & Pedley, 1996; Arenas et al., 2007). Tufa fragments, derived from the breakup of earlier phytoherm frameworks (Pedley, 1990) caused by moderate energy events that affected the paludal environment, accumulate around phytoherms in a static water body, as suggested by the lack of preferential organisation or orientation. Oncoids (facies C13) generally formed in slow-flowing waters in channels and dammed areas (Arenas et al., 2003). The phytoclasts of facies C12 were derived from the breakup of pre-existing tufa that may have formed micritic intraclasts. These components were carried during flood events that affected previous deposits formed in ponds and palustrine areas and then deposited in channels that linked different water bodies (Vázquez-Urbez et al., 2012).

5. Review of floral and faunal data

A review of previously published floral and faunal data from the Mytilini is proposed to complete the facies analysis.

5.1. Palynological data

Palynological data are available from three stratigraphic intervals and from different locations in the Mytilini Basin (Ioakim & Solounias, 1985; Ioakim et al., 2005; Ioakim & Koufos, 2009; Koufos et al., 2011): 1) the base of the Pythagorion Formation sampled in the Mavratzei section; 2) the middle part of the Hora

Formation (dominated by facies C9), sampled in the Hora section; 3) the Main Bone Beds Unit of the Mytilini Formation, sampled in the Mytilini section. Each of these intervals corresponds to a distinct floral assemblage.

The palaeovegetational material of the base of the Pythagorion Formation (FLA1; Figure 9; Ioakim & Solounias, 1985; Ioakim et al., 2005; Ioakim & Koufos, 2009) is dominated by arboreal pollen grains: *Mimosaceae* for the megathermic elements, as well as *Taxodiaceae* (*Taxodium*) and *Juglandaceae* (*Engelhardia*, *Myrica*) for the mega-mesothermic elements. Deciduous trees are well-expressed with *Quercus*, *Carya*, *Eucommia*, *Ulmus/Zelkova* and *Juglans*. Riparian plants, dominated by *Alnus*, *Salix* and *Cupressaceae* are also present, while thermophyllous evergreen species are rare. The herb pollen grains mainly exhibit *Amaranthaceae-Chenopodiaceae*, *Gramineae* and *Compositae*.

The floral assemblage for the middle part of the Hora Formation (FLA2; Figure 9; Ioakim et al., 2005; Ioakim & Koufos, 2009) is characterised mainly by mega-mesothermic elements, like *Engelhardia*, *Taxodiaceae*, *Hamamelidaceae*, *Nyssa*, *Myrica* and *Sapotaceae*. An increase in mesothermic elements (*Carya*, *Pterocarya*, *Cathaya*, *Ulmus/Zelkova*, *Acer*, *Carpinus*, *Symplocos*, *Betulaceae*, *Fagaceae*) is also observed. The herb assemblage is less compared to FLA1.

Finally, in the Mytilini Formation, a third floral assemblage (FLA3; Figure 9; Ioakim et al., 2005; Ioakim & Koufos, 2009) is observed. It shows a dominance of open vegetation plants like *Polygonaceae* (*Calligonum*) and *Poaceae* (*Lygeum*), as well as herbs like *Compositae* and *Amaranthaceae-Chenopodiaceae*. It is also characterised by the appearance of steppe elements like *Artemisia* and *Ephedra*, and by the absence of aquatic plants. Mega-mesothermic species are still present in lower proportions (*Taxodium*, *Engelhardia* and *Quercus)*, whereas the thermophyllous and xerophytic arboreal pollen shows high abundance (*Olea*, *Cistus* and *Quercus ilex*-type).

5.2. Diatom data

Owen et al. (2011) proposed a characterisation of the diatom floras existing in the Hora and uppermost part of the Pythagorion Formations in the Mytilini Basin. The main characteristics of these floras are recalled here (Figure 9).

In the south-eastern part of the Mytilini Basin (Hora section), in the uppermost metres of the Pythagorion Formation, very rare and corroded *Cyclotella aegaea* are present. The base of the Hora Formation is characterised by a low-diversity flora, dominated by *Nitzschia frustulum* (Kützing) Grunow and *Cyclotella aegaea*. The rare occurrences of *Epithemia turgida* (Ehrenberg) Kützing, *Tryblionella granulata* (Grunow) D.G. Mann, *Encyonema silesiacum* (Bleisch) D.G. Mann, *Diploneis ovalis* (Hilse) Cleve and *Cocconeis placentula* Ehrenberg are also described (Owen et al., 2011).

In the Mavratzei and Kavouraki sections (West of the Mytilini Basin), the diatom floras are of low diversity, but change gradually from the base to the top of the Hora Formation. The basal part is dominated by *Cyclotella aegaea*, with a small fraction of *Cyclotella aegaea var. pythagoria* Economou-Amilli. The occurrences of benthic taxa including *Diploneis ovalis* or *Achnanthes cf. miocoenica* are observed. The Middle part of the Hora Formation is dominated by a variety of *C. aegaea*, associated with *C. aegaea var. pythagoria*. *Nitzschia frustulum*, *Diploneis ovalis* and *Cocconeis placentula* may represent up to 4% of the samples. Finally, the upper part of the Hora Formation is characterised by *Cyclotella/Nitzschia*-dominated assemblages. Rare occurrences of *Diploneis ovalis*, *Synedra ulna*, *Cocconeis placentula*, *Nitzschia palea* (Kützing) W. Smith, *Tryblionella granulate, and rare minor species* may occur (Owen et al., 2011).

5.3. Gastropods

Five gastropod taxa have been identified in the succession of the Mytilini Basin. In the Pythagorion Formation outcropping in the Mavratzei-Kavouraki area, *Planorbis*, *Lymnaea* and *Bithynia* were identified by Koufos et al. (2011) or Ioakim and Koufos (2011). Owen et al. (2011) identified *Hydrobia* in the first half of the Hora Formation. Weidmann et al. (1984) described freshwater gastropods (probably *Planorbis*) in the White Beds Unit of the Mytilini Formation and "land gastropods" in the Main Bone Beds Unit. Finally, Koufos et al. (2011) and Ioakim and Koufos (2011) mentioned occurrences of *Brotia cf. graeca* in the Kokkarion Formation.

6. Geochemical data

6.1. Carbon and oxygen stable isotopes

The results of O and C isotope analyses are reported in Table S1 (supplementary material) and have been plotted alongside sedimentary columns (Figure 10) and in cross-plots of $\delta^{18}O$ versus $\delta^{13}C$ values (Figure 11). Four sections were sampled, the Kavouraki, Hora and Stephania sections from the Mytilini Basin and the Marathokampos section for the Karlovassi Basin.

In the Pythagorion Formation, the C and O analyses for original micrite mainly occupy the top left quarter of the cross-plot (Figure 11) and show a high variability, with values of $\delta^{18}O$ falling between -11.71 ‰ to 2.34 ‰ and values of $\delta^{13}C$ between -0.12 ‰ to +7.24 ‰ (Figure 10). However, each section shows a unique distribution. In the Kavouraki section, isotopic values are characterised by an apparent covariant trend between $\delta^{13}C$ and $\delta^{18}O$ values (correlation

coefficient is 0.90; Figure 11) with highly variable $\delta^{13}C$ values (from -0.12 ‰ to +6.62 ‰) but a narrower range of $\delta^{18}O$ values (from -8.98 ‰ to -5.25 ‰). No vertical trend is observed, but the highest values are preferentially associated with facies C3 and C4, whereas the lowest ones are associated with facies showing pedogenesis (C1 and C2). The analyses for the Hora section show a moderate negative covariance (correlation coefficient r^2=-0.71; Figure 11), with two groups of values: one with negative $\delta^{18}O$ values, and high $\delta^{13}C$ ones (up to +5.03 ‰) and the other with positive $\delta^{18}O$ values and lower $\delta^{13}C$ ones. No clear vertical trend is observed. Finally, in the Marathokampos section, isotopic values do not show any good covariance (correlation coefficient r^2=–0.47; Figure 11). The upper part of the formation shows slightly higher $\delta^{18}O$ values and lower $\delta^{13}C$ ones (although remaining positive).

In the Hora Formation, the C and O analyses occupy the top left quarter of the cross-plot (Figure 11) and show a narrower range of $\delta^{18}O$ values, with less negative values (from -8.46 ‰ to 0.92 ‰), with a more homogeneous distribution (Figure 10). No good covariance was observed in any section (Kavouraki r^2=0.26; Hora r^2=0.17; Marathokampos r^2=0.62). In the Kavouraki and Hora sections, the dolomitic facies at the base of the formation show the highest values of both $\delta^{18}O$ and $\delta^{13}C$ (Figure 10). The uppermost part of the formation, characterised by shallower facies, show a marked decrease of $\delta^{13}C$ values but no variation of $\delta^{18}O$ values. No clear vertical trend is observed for the Marathokampos section (Figure 10).

The Mytilini Formation is characterised by large variability of the isotopic signatures, with values of $\delta^{18}O$ between -10.36 ‰ to -3.96 ‰, and those of $\delta^{13}C$ between -4.81 ‰ to +5.27 ‰ (Figure 10). This variability is well expressed stratigraphically. The Old Mill Beds Unit is characterised by low $\delta^{18}O$ values (from -8.02 ‰ to -6.62 ‰) and $\delta^{13}C$ ones dominantly around 0 ‰ (from -1.26 ‰ to 1.02 ‰). The Gravel Bed Unit, White Bed Unit and Main Bone Beds Unit show less negative $\delta^{18}O$ values (from -8.20 ‰ to -3.96 ‰) and dominantly positive $\delta^{13}C$ values (from -0.15 ‰ to +5.27 ‰). Finally, the Marker Tuffs Unit displays

the most negative $\delta^{18}O$ (from -10.36 ‰ to -6.54 ‰) and $\delta^{13}C$ values (from -4.66 ‰ to -0.13 ‰). A moderate positive covariance is observed for the Stephania section, with samples from the Main Bone Beds and Marker Tuffs (r^2=0.78; Figure 11).

Finally, the Kokkarion Formation is characterised by a clustered distribution with good negative covariance (Stephania r^2=-0.87; Marathokampos r^2=-0.89; Figure 11). The two sections show the same distribution pattern, with a similar range of $\delta^{18}O$ values, but the Marathokampos section exhibits lower $\delta^{13}C$ values (from -1.42 ‰ to -5.76 ‰) than the Stephania section (from 0.92 ‰ to -2.32 ‰).

6.2. Strontium isotopes

The results of Sr isotope analyses are reported in Table S1 (supplementary material) and have been plotted against age and stratigraphy (Figure 12). Most of the $^{87}Sr/^{86}Sr$ ratios range from 0.707879 to 0.708168, significantly lower than the range of contemporaneous marine influenced carbonates (McArthur & Howarth, 2004), which argue in favour of a continental origin for the waters. All the $^{87}Sr/^{86}Sr$ ratios obtained in the Marathokampos section (Karlovassi Basin) fall in this range of values. In the Kavouraki section, two points, located at the beginning of the Pythagorion and the Hora formations (0.70872 and 0.708487, respectively) are out of the trend. The same pattern is observed in the Hora sections for three points (0.708601, 0.708502 and 0.708558) also localised at the beginning of these two formations. The highest values are comparable to the marine seawater values of McArthur and Howarth (2004). Whatever the section, the $^{87}Sr/^{86}Sr$ ratios of the middle and upper part of the Mytilini Formation are slightly higher than the general trend (from 0.708132 to 0.708329).

7. Discussion

7.1. Evolution of the depositional environments, lake chemistry and hydrology

7.1.1. Basal Conglomerate and Pythagorion formations

The basin-fill succession begins with the deposition of the Basal Conglomerate Formation, overlying unconformably the pre-Neogene basement. In the Mytilini Basin, the Basal Conglomerate is present in the whole area. Two types of facies association can be found. In the western part of the basin (Pyrgos section; Figure 3), FA1 (fan-derived alluvial facies association) is dominant. This facies association suggests a subaerial alluvial system (distal reaches of alluvial fans) located in the Pyrgos sub-basin and supplied with sediments from the central basement ridge forming a prominent relief (Weidmann et al., 1984). In the centre of the basin (Hora and Paghondas sections; Figure 3), the occurrence of FA2 (stream-derived alluvial facies association), its lateral extent, as well as the few current directions indicating N-S and NW-SE flow directions suggest more likely a braided plain environment (comparable to the megafan systems described by Leier et al., 2005, and Schmitz & Pujalte, 2007), supplied from the north, and laterally fed in the west by alluvial fans that developed on the basin margin (Kavouraki and Mavratzei sections). In the Karlovassi Basin (Figure 3), the Basal Conglomerate Formation is dominated by FA1 which indicate fan-derived alluvial environments, at least in the southern part of the basin (Marathokampos section). These deposits developed under the subtropical and humid conditions of the Serravallian stage (Ioakim et al., 2005), which favoured basement erosion and the supply of terrigenous material to the basin.

The overlying deposits suggest the development of shallow, low-energy palustrine to lacustrine conditions, but with various characteristics depending on the location. In the western part of the Mytilini Basin (Figure 3), the Basal Conglomerate Formation gradually evolves toward FA3 (marginal palustrine facies

association), indicating a periodically emerged lake-margin zone hosting a low-relief palustrine environment (Freytet & Verrecchia, 2002). These deposits are rich in plant debris and gastropods (*Planorbis*, *Lymnaea* and *Bithynia*) that suggest slowly running, fresh to slightly brackish water of lakes and marshes (Neubert, 1998; Juřičková et al., 2001; Armenteros & Edwards, 2012) (Figure 13A). Carlsson (2006) described *Lymnaea* and *Bithynia* in brackish water up to 6 g/L, with a pH value between 7.6 and 9.7 (moderately basic). This environment is consistent with the floral assemblage FLA1, characterised by the presence of riparian and water-dependent plants (*Osmundaceae*, *Nymphaeaceae* and *Typhaceae*), typical of freshwater wetlands (Collinson, 2002). Moreover, the abundance and diversity of arboreal pollens found in FLA1 are indicative of mixed-mesophytic forest developing under subtropical to warm temperate conditions with high humidity (Ioakim & Solounias, 1985; Ioakim & Koufos, 2009). The well-expressed covariant trend between $\delta^{18}O$ and $\delta^{13}C$ values (Figure 11) observed for the Kavouraki section suggests carbonates precipitating from water with relatively long residence time in a hydrologically closed system (Hillaire-Marcel & Casanova, 1987; Talbot, 1990). This covariance together with the narrow range of $\delta^{18}O$ values suggest an important variability of the lake waters: during humid periods, a positive inflow/evaporation balance and the dense vegetation cover in the catchment area, respectively, led to the depletion in $^{18}O_{water}$ and $^{13}C_{DIC}$, whereas dry periods with negative inflow/evaporation balance favoured $^{13}C_{DIC}$ and $^{18}O_{water}$ (Lettéron et al., 2017). The end of the Pythagorion Formation is marked by the deposition of a 10 to 30 m thick basalt flow (observed in the Paghondas, Mavratzei and Kavouraki sections; Figure 3) followed by a thick (several tens of metres) tuff layer (facies V2).

In the south-eastern part of the Mytilini Basin, sedimentary facies are more diverse: FA3 is less well represented, whereas FA4 (lacustrine sublittoral facies association) is dominant (Figure 3). Depositional environments range from palustrine domain to shallow littoral and low-energy distal, sublittoral domains (Figure 13A). The presence of the salinity tolerant gastropod *Hydrobia* (reported from quiet estuaries, coastal marshes and saline lakes) and the absence of purely freshwater fauna may point to brackish water or a variable salinity (Casagranda et al., 2005). The moderate negative covariance between $\delta^{18}O$ and $\delta^{13}C$

values (Hora section) could indicate an enrichment of ^{18}O and ^{12}C, explained by a decrease in the freshwater input associated with an evaporative effect and an increase of organic productivity, respectively (Utrilla et al., 1998; Alçiçek & Jiménez-Moreno, 2013). An alternative explanation is the possible contamination of the lake water with episodic incursions of marine-related water or groundwater inflows (Lettéron et al., 2018). Indeed, a few points of the dataset are close to values of marine calcite of Serravallian-Tortonian age (Figure 11). This hypothesis is also supported by the $^{87}Sr/^{86}Sr$ ratios that show intermediate values between meteoric and marine waters, at the beginning of the Pythagorion Formation, in both the Kavouraki and the Hora sections. This may suggest a mixing of water of different origins of marine and non-marine waters (Ligios et al., 2012). Under the warm temperate and highly humid climate at that period, such episodic connections with marine-related waters could finally explain the origin of salinity in this lake.

In the south of the Karlovassi Basin (Marathokampos section; Figure 3), the equivalent Pythagorion Formation displays the facies association FA3. Palustrine to shallow marginal lacustrine conditions are therefore inferred. However, the isotopic dataset does not show any good covariance, which suggests a hydrologically opened system and humid conditions (Talbot, 1990). The positive $\delta^{13}C$ values (from +3.00 to +6.92 ‰) may be explained by a ^{13}C uptake related to photosynthetic activity and the leaching of the basement marbles in the catchment area (Lettéron et al., 2018). Indeed, the marbles of Fourni Island (south-westward of Samos) typically display positive $\delta^{13}C$ values (Lazzarini & Cancelliere, 2000). and may have resulted in ^{13}C–enriched HCO_3^- waters. The large range of $\delta^{18}O$ values (from −11.71 to −5.83 ‰) associated with a lesser variability of $\delta^{13}C$ values may point to dryer periods with negative inflow/evaporation ratios (Talbot, 1990; Arenas et al., 1997; Lettéron et al., 2018). No salinity indicators were found within the Marathokampos section, but Stamatakis et al. (1989) interpreted saline and alkaline conditions, further north.

These differences between basins and between areas of the same basin point to the existence of several separate or partially separate lake water bodies, with possible episodic connections between them. Possible connection of the lake system with a neighbouring marine-influenced water body is inferred in the Mytilini Basin at the base of the Pythagorion Formation.

7.1.2. Hora Formation

In the Mytilini Basin, the Hora Formation conformably overlies the previous deposits and starts (Unit 1) with the alternation of facies association FA5 (marginal evaporative) and FA4 (lacustrine sublittoral) (Figure 3. This pattern records water level fluctuations, causing the development of hypersaline shallow marginal environments and episodic desiccation (Figure 13B). The positive $\delta^{18}O$ and $\delta^{13}C$ values observed for the dolomitic facies indicate enrichment both in ^{18}O and ^{13}C. Assuming equilibrium precipitation, this may indicate that the dolomite precipitated from water with relatively long residence times associated with a low precipitation/evaporation ratio, under evaporitic conditions (Gasse et al., 1987; Hillaire-Marcel & Casanova, 1987). These interpretations are consistent with the diatom floras (dominated by *Cyclotella aegaea* and *Nitzschia frustulum*; Owen et al., 2011) that indicate alkaline and saline conditions (Trobajo et al., 2004; Kociolek & Khursevich, 2013), as well as the presence of *Hydrobia*. They are also supported by the $^{87}Sr/^{86}Sr$ ratios, observed at the base of the Hora Formation, which, again, point to a mixing of marine and non-marine waters (Ligios et al., 2012). Such deposits were not observed in the Marathokampos section (Karlovassi Basin; Figure 3) where FA4 is dominant, with $^{87}Sr/^{86}Sr$ ratios indicative of the water continental origin. Stamatakis et al. (1989) interpreted saline and alkaline conditions, further north. This may point to separate basins, with different hydrological conditions. This environmental evolution is accompanied, from Unit 1 to Unit 2 (Figure 3), by changes in the physiography of the basins, marked by synsedimentary deformations (slumps, convolute; facies C5b) in a

period of tectonic instability (Owen et al., 2011). This seems to have generated a high subsidence and the formation of sedimentary slopes that separate proximal shallow margins from a distal deep offshore domain (Figure 13B).

Units 2 and 3 (Figure 3) are characterised by homogenisation of the sedimentary pattern, with the occurrence of FA6 (lacustrine profundal facies association), and a lack of subaerial exposure, which suggest offshore and relatively deep perennial lacustrine conditions, in both basins. The lack of covariant trends between $\delta^{18}O$ and $\delta^{13}C$ values, and the similar range of values for the three sections (Marathokampos, Kavouraki, Hora) also suggest a hydrologically open system (Talbot, 1990) with a significant lake expansion that connected the pre-existing isolated water bodies, and the two main basins through the Pyrgos sub-basin. The narrow range and negative $\delta^{18}O$ values of calcite (−8.46 ‰ to −2.56 ‰) suggest ^{16}O-rich meteoric waters due to subhumid conditions (Bustillo et al., 2002; Alçiçek & Jiménez-Moreno, 2013). This is in agreement with the low $^{87}Sr/^{86}Sr$ ratios indicative of meteoric waters. The positive and variable $\delta^{13}C$ values can be explained by the ^{13}C uptake due to the high development of photosynthetic diatoms (McKenzie, 1985). The diatom assemblage, dominated by *C. aegaea* and variants (*Cyclotella sp. 1*, *C. aegaea var. pythagoria*) may also indicate more dilute and brackish conditions compared to Unit 1 (Owen et al., 2011).

Finally, the top of the Hora Formation (Unit 4) is marked by a gradual shallowing-upward trend, from FA6 (lacustrine profundal facies association) to FA4 (lacustrine sublittoral facies association) and FA3 (marginal palustrine), well exposed in the Kavouraki section (Figure 3). The relatively constant and negative $\delta^{18}O$ values (−7.56 ‰ to −6.24 ‰) indicate the input of ^{16}O-rich meteoric waters, consistent with the low $^{87}Sr/^{86}Sr$ ratios. The upward decreasing trend in $\delta^{13}C$ values (from +5.75 ‰ to -0.61 ‰) may reflect the progressive involvement of isotopically light CO_2 derived from biological processes related to the swamp vegetation in the palustrine domain (Huerta & Armenteros, 2005; Lettéron et al., 2018). This is in line with the floral assemblage FLA2 which suggests a

homogeneous vegetation of a widespread and dense woodland developing mainly under temperate and moderate humidity conditions (Ioakim & Koufos, 2009), coeval with a slight deterioration in climate with cooler and drier conditions than previously (Koufos et al., 2011).

The diatom flora characterised by multiple species with a large range of salinity (from fresh to brackish water) and the co-occurrence of *Hydrobia* and *Lymnaea* also suggest fresher conditions than before. The occurrences of *Encyonema silesiacum* (Bleisch) D.G. Mann and *Diploneis ovalis* (Hilse) Cleve are indicative of freshwater species adapted to arid environments (Aboal et al., 2003; John, 2020).

This unit is capped by a major angular unconformity that seems to erode the upper part of the Hora Formation (Unit 4). This surface also indicates complete desiccation of the lake and the exposure of the succession (Weidmann et al., 1984).

7.1.3. Mytilini Formation

In the Mytilini Basin, the Mytilini Formation overlies unconformably the top of the Hora Formation. It is characterised by terrigenous alluvial sedimentation involving different processes and environments (Figure 4). The Old Mill Beds Unit is composed of facies association FA2 and reflects an alluvial plain with fluvial channels, on which volcanic tuffs are deposited and preserved. The Gravel Bed Unit is dominantly made up of facies association FA1, indicative of a high energy fan-derived alluvial environment (Figure 13C). This evolution suggests a change in the flow regime, pointing towards more contrasted seasons with recurrent important flooding episodes reactivating an ephemeral braided plain environment (Miall, 1977; Rust, 1978). The few carbonate beds sampled for isotope analyses show values similar to the end of the Hora Formation with relatively constant and negative $\delta^{18}O$ values typical of meteoric waters (Huerta

& Armenteros, 2005; Alçiçek & Jiménez-Moreno, 2013). The low $\delta^{13}C$ values (most around 0‰) may be due to a mixture of atmospheric and soil-derived CO_2 from the surrounding catchment (Sáez & Cabrera, 2002; Alçiçek & Jiménez-Moreno, 2013).

The White Beds Unit is characterised by the alternation of fine-grained muddy facies associations FA1 and FA3 (Figure 4). The presence of palustrine carbonate facies (FA3) may point to localised freshwater (*Planorbis*) ephemeral ponds developed on an alluvial plain (Figure 13C). The Main Bone Beds Unit and the Marker Tuffs Unit are dominated by facies association FA2 (stream-derived alluvial) and are characteristic of an alluvial plain with fluvial channels, with less development of palustrine facies (FA3) indicative of dryer conditions and increasing volcanic activity at the end of the formation, explaining the important accumulation of volcanic tuffs (V1 and V2). The occurrence of facies T4 (unchannelised sheetfloods) may also point to dry conditions with episodic flood events (Figure 13C). This is in agreement with the floral assemblage FLA3, sampled in the Main Bone Beds Unit, that indicates open vegetation rich in herbs developed under drier conditions compared to the previous assemblages (Ioakim & Koufos, 2009). Alçiçek and Jiménez-Moreno (2013) even described a semiarid climate in the Karacasu Basin (SW Turkey). The isotopic analyses also show a different pattern than previously, with a wide variability of $\delta^{18}O$ and $\delta^{13}C$ values and no evident trends. This can be explained by the ephemeral character of the water bodies giving rise to facies C1 and C2, and highly variable hydrological conditions.

In the Karlovassi Basin, it was not possible to recognise the stratigraphic subdivisions defined in the Mytilini Basin (Figure 4). The succession is dominated by facies association FA2, with abundant volcaniclastic tuff (V1 and V2) and floodplain facies (T5), and rare occurrences of fluvial channels (T2 and T3). The isotopic measurements show a similar erratic pattern, with no specific trend. The $^{87}Sr/^{86}Sr$ ratios measured for the Mytilini Formation are slightly higher than the general trend inferred for continental meteoric waters. This enrichment in ^{87}Sr may be related to the interaction between meteoric fluids and the high amount of volcanic material present in this formation providing more radiogenic strontium (Rhodes et al., 2002).

7.1.4. Kokkarion Formation

The Kokkarion Formation overlies conformably the Marker Tuffs Unit (Weidmann et al. 1984). The presence of intercalated clays (T5) and marls (C1) in the basal part of the Kokkarion Formation indicates a progressive transition, with no discontinuity. The facies are similar in both basins (Figure 4). This formation is classically interpreted as travertine deposits (Weidmann et al., 1984; Stamatakis et al., 1989), but recent works (Bailly, 2019) have interpreted this formation as typical of a paludal tufa system (Pedley, 1990).

The sedimentary facies analysis shows the coexistence of three palaeoenvironments (Figure 13D): an alluvial plain with local ephemeral ponds (FA2, only observed in the Pythagorion section; Figure 4), passing laterally to a palustrine domain (FA3) and marshes colonised by Phragmites (FA7) (Bailly, 2019). Such facies are typical of poorly drained, humid areas in which a mixed flora and fauna develop and become heavily encrusted by fringe cements (Pedley, 1990). The presence of the gastropod *Brotia cf. Graeca* is also indicative of a shallow (less than 2 m), freshwater environment developed under a humid climate (Báldi, 1973; Willmann, 1981), which is consistent with the low $^{87}Sr/^{86}Sr$ ratios. No palynological data were available for the Kokkarion Formation. However, based on the Zanclean deposits of Crete, Ioakim et al. (2005) described a subtropical climate, a little more humid than in the Miocene. Alçiçek and Jiménez-Moreno (2013) also described a subhumid climate in neighbouring south-western Anatolia.

The isotopic values are all in the same trend and show good negative covariance that may reflect post-depositional palustrine alteration processes (Boulton et al., 2019). The negative $\delta^{18}O$ values suggest ^{16}O-rich meteoric waters (Alçiçek & Jiménez-Moreno, 2013) and the dominantly negative $\delta^{13}C$ values suggest involvement of isotopically light CO_2 derived from biological processes related to the marsh vegetation. The lower $\delta^{13}C$ values observed in the Marathokampos

section may be interpreted as ^{12}C-enriched soil-derived meteoric water coming from the surrounding catchment or groundwater (Dunagan & Turner, 2004), due to a more proximal position than the Stephania section, localised in the middle of the Mytilini Basin.

7.2. Structural considerations

The initiation of the Mytilini and Karlovassi sedimentary basins of Samos in Serravallian times and their evolution throughout the Late Miocene seems to be mainly controlled by N-S to NNE-SSW striking faults (Ring et al., 1999; Pe-piper & Piper, 2007). Due to the lack of reliable kinematic indicators, the kinematic character of these faults is difficult to resolve convincingly. However, the geometrical relationship of the basin-bounding faults, the strike-slip character of the NNE-SSW striking transition zone between Western Turkey (Menderes Massif) and the Aegean domain (Roche et al., 2019), and the major extension direction parallel to the latter transition zone call for a style of deformation of the upper crust that is rather more complex than simple extension accommodated by normal faults. Different models for the tectonic development and evolution of the sedimentary basins of Samos in the Late Miocene can be considered (Figure 14).

The first model (Figure 14A) is compatible with the interpretation of Ring et al. (2017) who proposed the existence of a sinistral strike-slip corridor (East Aegean transition zone) which accommodated the differential extension between Western Turkey (Menderes Massif) and the faster extending Aegean domain. This wrench component is superimposed on the regional NNE extension by translation across a diffuse plate boundary (Ring et al., 2017). In this hypothesis, a 20° counterclockwise rotation since the Late Miocene is supposed. En echelon arranged highly oblique to strike-slip sinistral faults striking NE-SW associated with NW-SE striking normal faults produce local extension and lead to the creation of the Karlovassi and Mytilini pull-apart basins.

The second model (Figure 14B) is based on the interpretations of Roche et al. (2019), who conclude that the slab retreat related extension in the East Aegean transition zone maintains a constant NNE-SSW direction while the observed deformation is accommodated by low-angle normal faults and ductile shear zones, without clear evidence for large-scale strike-slip fault systems that could have been expected above a slab tear. This interpretation coincides with the suggestions of Gessner et al. (2013) and Jolivet et al. (2015) on a diffuse gradient of crustal extension, accommodating the left-lateral displacement imposed by the faster retreat south of the Aegean Sea in respect to the Menderes Massif. This model implies a 30° counterclockwise rotation affecting the continental blocks of the East Aegean and part of the Menderes Massif (Kissel & Laj, 1988; Van Hinsbergen, 2010; Jolivet et al., 2015). On Samos (Figure 14B), major, NE-SW striking, dextral strike-slip faults and conjugate, NNW-SSE striking, sinistral strike-slip faults accompanied by NW-SE striking normal faults produce local extension in a NNE-SSW direction and have accommodated the initiation and evolution of the Late Miocene sedimentary basins.

The post-Miocene deformation of the Aegean domain, including Samos (Figure 14C), results from the interaction of the gradual westward extrusion of the Anatolian Block and the acceleration of the slab retreat below the Aegean. The propagation of the North Anatolian Fault in the Aegean domain in the Early Pliocene (Armijo et al., 1996, 1999) or even later in Late Pliocene to Middle Quaternary (Beniest et al., 2016; Ferentinos et al., 2018; Tsampouraki-Kraounaki et al., 2021) marks the acceleration of the NNE-SSW stretching of the Aegean domain and enhanced shearing in a NE-SW to ENE-WSW direction (Sakellariou & Tsampouraki-Kraounaki, 2019).

7.3. Regional palaeoenvironmental implications

Based on the spatial and temporal evolution of the sedimentary systems occurring in the Samos basins, and their comparison with neighbouring basins, it is possible to open a new window to the understanding of the forcing parameters on the sedimentation (Figure 15).

7.3.1. Serravallian to Early Tortonian

As described previously, the initial development of the Samos basins date from the late Serravallian (around 12 Ma) and coincides first with the end of a crustal extensional phase that began in the Oligocene (D3 of Ring et al., 1999) and, second with the tearing of the subducting slab below the Eastern Aegean and Western Turkey between 15 and 8 Ma (Jolivet et al., 2015). The subsidence occurs mainly along basin-margin strike-slip faults striking NE-SW, with apparent correlative faults in the marine areas south of the Karaburun Peninsula (Ocakoğlu et al., 2004, 2005; Pe-piper & Piper, 2007). These faults may have facilitated the flow of magmatic fluids and have largely controlled the spatial distribution of alkaline volcanic rocks along the eastern margin of the Karlovassi Basin and the western margin of the Mytilini Basin. Pe-Piper and Piper (2007) interpreted these features as indicative of large-scale strike-slip faulting, that also occurred in the islands of Chios and Kos, but also in Western Anatolia, from the Late Tortonian until the Early Pliocene (Yılmaz et al., 2000; Kaya et al., 2004; Göktaş, 2014). Finally, the Pyrgos area is interpreted as a half-graben bounded by a WNW–ESE striking master fault.

During the deposition of the Basal Conglomerate and Pythagorion formations, the subsidence seems relatively slow and regular, as the depositional environments remain shallow, water bodies are isolated from each other and no major break in the sedimentation occurs. The Late Serravallian – Early Tortonian subtropical to warm temperate and highly humid climate (Ioakim et al., 2005), favours the development of freshwater lakes and wetlands in such

extensional basins (Figure 15): It is the case further north in the Çeşme and Karaburun Peninsula (Göktaş, 2014; 2020) and in the South Saros Gulf (Sakinç et al., 1999), but also in south-west Anatolian basins like the Çameli Basin or the Denizli Basin (Alçiçek et al., 2005, 2007).

A peculiar question in the case of the Mytilini Basin is the hypothesis of episodic connections with marine-derived waters. At that period, the Northern Aegean region was separated from the Mediterranean in the south by the Cyclades sill that formed the main barrier for marine incursions (Meulenkamp, 1971; van Hinsbergen & Schmid, 2012). However, around 12 Ma, the fragmentation of this landmass began and led to the formation of the future Mid-Aegean Trench (fully accomplished by 10–9 Ma; Steininger & Rögl, 1984). Moreover, the Early Tortonian corresponds to a relatively high eustatic sea-level period (+60 m, cycle TB2.2.6 of Haq et al., 1987; Tari et al., 2016). This may have enabled brief influxes of marine water, as observed in the Gulf of Saros at this period (Sakinç et al., 1999; Krijgsman et al., 2020; Figure 15). Given the more southern position of the Samos basins compared to the Northern Aegean domain, such short-duration marine ingressions, through intermediate basins, are conceivable.

7.3.2. Middle Tortonian

The onset of the Hora Formation is marked by a major reconfiguration of the basins' morphology, with the development of deep depocentres and increasing subsidence during a period of active extensional tectonics. In the Mytilini Basin, several pulses of subsidence have been identified. Three main episodes (corresponding to Unit 1, Unit 2 and Units 3 and 4 of the Hora Formation, Figure 3) are characterised by a rapid deepening in the basin axis, followed by a progressive shallowing upwards of the depositional environments. These trends, associated with the synsedimentary deformation described above suggest short and abrupt tectonic pulses that generate subsidence, followed by a tectonic quiescence and basin infill sequences up to shallow marginal lacustrine

environments in the basin depocentre. This increasing subsidence may be associated with an increasing rotation rate of the West Aegean block that may have triggered (or enhanced) this deformation (Le Pichon & Angelier, 1981). Moreover, Brun et al. (2016) have proposed a significant acceleration of the slab retreat below the Aegean from 0.6 cm/yr during the Oligocene to Middle Miocene, to 1.7 cm/yr since 15 Ma, and to 3.2 cm/yr in the Plio-Quaternary. This acceleration can be explained by the tearing below the Eastern Aegean and Western Turkey.

The origin of such a transition seems to be of regional significance as many basins of the Aegean region are similarly affected; basin formation and initiation of the sedimentation in Kos Island (Böger et al., 1974; Willman, 1983); basin formation, initiation, and rapid transition from continental to marine sedimentation in Crete (Zachariasse et al., 2011), marine transgression in the South Saros Gulf (Sakinç et al., 1999) (Figure 15). On the other hand, this deepening phase is not observed in the western Anatolian basins (Alçiçek et al., 2005, 2007; Alçiçek, 2009). This is in line with the work of Ring et al. (1999) who showed that both regions underwent very different degrees of crustal stretching. This important and rapid subsidence coupled with the warm temperate and moderately humid conditions may explain the major expansion of the different isolated water bodies and their connections in a single major lake.

During this period (Hora Formation, Units 1 to 3), alkaline and saline water gave rise to evaporite precipitation and dolomitisation processes in the marginal environments of the lake. Similar features occurred coevally in the South Saros Gulf (Sakinç et al., 1999) and in the Denizli Basin (Alçiçek et al., 2007) (Figure 15), which can be related to dryer conditions and by increasing seasonality (Owen et al., 2011), with increasing summer droughts throughout Paratethys and the circum-Paratethys region (Butiseacă et al., 2021). Such severe droughts led to partial desiccation of the Paratethys megalake, between 9.75 and 9.6 Ma and between 9.5 and 9.3 Ma (Butiseacă et al., 2021; Palcu et al., 2021; Figure 15). This deterioration in climate is accompanied by a progressive rise in the

prevalence of grassy environments in the Eastern Mediterranean zone (Ioakim et al., 2005) that may have enhanced the production of terrestrial dissolved silica during the late Miocene, favouring the important development of diatoms in Samos lake (Pellegrino et al., 2018).

The end of the Hora Formation is marked by an erosional angular unconformity, dated around 9 to 8.6 Ma (Weidmann et al. 1984; Boronkay & Doutsos, 1994; D4 of Ring et al., 1999). An equivalent unconformity is observed in Kos Island and in the Çeşme and Karaburun Peninsula (Figure 15), indicating a regional event that also affected Western Anatolia (Yılmaz et al., 2000). Menant et al. (2013) and Roche et al. (2019), suggest that this short-lived regional compressional regime is linked to the very beginning of Anatolia extrusion. However, this transition is also marked by a gradual shallowing-upward trend and the development of palustrine conditions, prior to the unconformity. This period corresponds to one of the Paratethys regression episodes (between *ca* 9.0 and 8.7 Ma) and an important climate and palaeoenvironmental change, with the replacement of the European humid forest landscapes by dry, open woodland and grasslands, marking an increased aridity (Böhme et al., 2018; Palcu et al., 2021). Thus, a possible role forclimate on the progressive desiccation of the Samos lakes, prior to the unconformity cannot be totally discarded.

7.3.3. Late Tortonian to Messinian

Following crustal contraction, the basins were subjected to renewed subsidence with deposition of the thick (250 m in average) Mytilini Formation and important volcanism in the Karlovassi Basin (Koumeika rhyolite, Katavasis (or Kallithea) igneous complex). Pe-piper and Piper (2007) interpreted these features as indicative of large-scale strike-slip faulting, that also occurred in Western Anatolia, from the Late Tortonian until the Early Pliocene (Yılmaz et al., 2000; Kaya et al., 2004; Göktaş, 2014).

Despite this subsidence, the Samos basins are filled by terrigenous and volcaniclastic alluvial successions, rather than lacustrine sediments. The same pattern is observed in Kos Island, in the Çeşme and Karaburun Peninsula, and in the South Saros Gulf with slightly diachronous timing (Sakinç et al., 1999) (Figure 15). This suggests drier conditions, resulting from a deteriorating climate, that induced, low precipitation and river run-off but high evaporation, leading to an ephemeral alluvial system. Indeed, during the late Tortonian-early Messinian, in the peri-Mediterranean region, a general trend of cooling and seasonal aridification occurred from 8 Ma until 5.9 Ma (Tzanova et al., 2015; Böhme et al., 2018), culminating during the latest Miocene (MN13 - 6.6–5.3 Ma), when the Mediterranean region was at its driest (Eronen, 2006, 2009; Fortelius, 2006). The latter can be correlated to the MSC, recorded in the Mediterranean basins between 5.97 and 5.33 Ma (Krijgsman et al., 2010; Roveri et al., 2014; Flecker et al., 2015). Effects of the MSC differ by region, depending on palaeogeography, palaeoclimate and palaeotopography. For example, in the Northern Aegean region (Saros Gulf), marine carbonate deposited during the Late Tortonian to Early-Messinian are replaced abruptly by brackish sandstones and claystones of Late Messinian age (Sakinç et al., 1999; Sakınç & Yaltırak, 2005; Krijgsman, et al., 2020). This marks the transition between the Egemar Sea and the Egemar Lake (Krijgsman, et al., 2020), with a temporary loss of Mediterranean influence due to regression of the Mediterranean from the region, and supply of fresh to brackish water from the Paratethys (Sakınç & Yaltırak, 2005). In Samos (as well as in Kos or in the Cesme Peninsula; Figure 15), no peculiar sedimentary pattern or discontinuity is observed, which suggests a relative isolation of this region from the scenario described for the Northern Aegean region.

7.3.4. Zanclean

From the latest Miocene to the present, a new extensional deformation phase occurred (D5 of Ring et al., 1999), producing W/NW-striking faults. Some of them affect the Kokkarion succession, as in the Pythagorion area, where the outcropping section corresponds to a tilted block along a S-dipping normal fault. This extensional deformation seems to have generated a gentle and homogeneous subsidence as the depositional environment of the Kokkarion Formation remains unchanged and shallow all along the succession. The freshwater paludal palaeoenvironment is indicative of more humid conditions than during the previous period. This trend is observed regionally, in the Northern Aegean and Western Anatolian regions (Figure 15). Indeed, even if Early Pliocene precipitation decreased in Central Europe, warm and humid conditions were preserved in the Eastern Mediterranean region (Eronen et al., 2009; Alçiçek & Jiménez-Moreno, 2013), giving rise to swampy and shallow lacustrine freshwater systems (Figure 15). The end of the succession is supposed to be marked by an erosional surface (Weidmann et al., 1984), the origin of which remains unclear.

8. Conclusion

The Late Miocene to Pliocene continental sedimentary succession from Samos Island provides a complete record of the environmental perturbations associated with climate change and active tectonics. The palaeoenvironmental evolution recorded by this succession has been characterised by a detailed analysis, integrating sedimentological, palaeontological and geochemical data. Five main stages of basin evolution have been identified: 1) initiation of sedimentation marked by the development of a megafan fed by lateral alluvial fans and distally subaqueous; 2) a series of isolated or semi-isolated shallow lakes with variable salinity, from fresh to brackish, under warm and relatively humid conditions; 3) a large and deep lake with saline and alkaline waters, under

slightly colder and drier conditions; 4) an alluvial system, with an ephemeral fluvial dynamic, developed under a dry climate; 5) a palustrine and paludal wetland system, dominated by tufa carbonates, developed under moderately humid conditions.

The climate variability of the Late Miocene to Pliocene remarkably controls the depositional record found in Samos and its neighbouring regions. The dataset supports a detailed depositional record of the deteriorating Late Miocene climate. This change started in the Early Tortonian with an increasing seasonality and more and more arid conditions, culminating during the Messinian period with the replacement of the lacustrine systems by alluvial ones. Finally, during the Early Pliocene, more humid conditions prevail, promoting the regeneration of freshwater swamps. The Samos succession also records the large-scale effect of the geodynamic evolution of the Eastern Aegean zone, through significant subsidence, interrupted in the mid-Tortonian (9 Ma) by a brief compressive event.

The origin of the salinity in these lacustrine environments could be due to episodic ingressions of marine-related water or groundwater inflows, as suggested by the geochemical data and the presence of flora (diatoms) and fauna (gastropods) of marine affinity. This is line with marine connections described further north for the same period.

9. References

Aboal, M., Álvarez Cobelas, M., Cambra, J., Ector, L. (2003) *Floristic list of non-marine diatoms (Bacillariophyceae) of Iberian Peninsula, Balearic Islands and Canary Islands.* Diatom Monographs, 4, A.R.G. Gantner Verlag K.G.

Ainsworth, R.B., Hasiotis, S.T., Amos, K.J., Krapf, C.B.E., Payenberg, T.H.D., Sandstrom, M.L., Vakarelov, B.K., Lang, S.C. (2012) Tidal signatures in an intracratonic playa lake. *Geology*, 40(7), pp. 607–610. https://doi.org/10.1130/G32993.1Alçiçek, H. (2009) Late Miocene nonmarine sedimentation and formation of magnesites in the Acıgöl Basin, southwestern Anatolia, Turkey. *Sedimentary Geology*, 219(1-4), 115–135. https://doi.org/10.1016/j.sedgeo.2009.05.002

Alçiçek, H., Jiménez-Moreno, G. (2013) Late Miocene to Plio-Pleistocene fluvio-lacustrine system in the Karacasu Basin (SW Anatolia, Turkey): Depositional, paleogeographic and paleoclimatic implications. *Sedimentary Geology*, 291, 62–83. https://doi.org/10.1016/j.sedgeo.2013.03.014

Alçiçek, M.C., Kazancı, N., Özkul, M. (2005) Multiple rifting pulses and sedimentation pattern in the Çameli Basin, southwestern Anatolia, Turkey. *Sedimentary Geology*, 173(1–4), 409–431. https://doi.org/10.1016/j.sedgeo.2003.12.012

Alçiçek, H., Varol, B., Özkul, M. (2007) Sedimentary facies, depositional environments and palaeogeographic evolution of the Neogene Denizli Basin, SW Anatolia, Turkey. *Sedimentary Geology* 202(4), 596–637. https://doi.org/10.1016/j.sedgeo.2007.06.002

Alonso-Zarza, A.M. (2003) Palaeoenvironmental significance of palustrine carbonates and calcretes in the geological record. *Earth-Sciences Reviews*, 60(3-4), 261–298. https://doi.org/10.1016/S0012-8252(02)00106-X

Alonso-Zarza, A.M., Meléndez, A., Martín-García, R., Herrero, Mª J., Martín-Pérez, A. (2012) Discriminating between tectonism and climate signatures in palustrine deposits: Lessons from the Miocene of the Teruel Graben, NE Spain. *Earth-Science Reviews*, 113(3–4), 141-160. https://doi.org/10.1016/j.earscirev.2012.03.011.

Arenas, C., Cabrera, L., Ramos, E. (2003) Fluvial-lacustrine microbialites from the Cala Blanca Formation (Oligocene, Mallorca, Western Mediterranean). In: Valero-Garcés. B.L. (Ed.) *Limnogeology in Spain: A tribute to Kerry R. Kelts*. Consejo Superior de Investigaciones Científicas (CSIC), Colección Biblioteca de Ciencias, 119-150.

Arenas, C., Cabrera, L. and Ramos, E. (2007) Sedimentology of tufa facies and continental microbialites from the Palaeogene of Mallorca Island (Spain). *Sedimentary Geology*, 197, 1–27. https://doi.org/10.1016/j.sedgeo.2006.08.009

Arenas, C., Casanova, J., Pardo, G. (1997) Stable-isotope characterization of the Miocene lacustrine systems of Los Monegros (Ebro Basin, Spain): palaeogeographic and palaeoclimatic implications. *Palaeogeography, Palaeoclimatology, Palaeoecology*, 128, 133–155. https://doi.org/10.1016/S0031-0182(96)00052-1

Armenteros, I., Daley, B., García, E. (1997). Lacustrine and palustrine facies in the Bembridge Limestone (late Eocene, Hampshire Basin) of the Isle of Wight, southern England. *Palaeogeography, Palaeoclimatology, Palaeoecology*, 128(1–4), 111–132. https://doi.org/10.1016/S0031-0182(96)00108-3

Armenteros, I., Edwards, N. (2012) Palaeogeographic, palaeoclimatic, palaeohydrological and chemical/biochemical controls on accumulation of late Eocene coastal lacustrine-palustrine limestones, Southern England. *Sedimentary Geology*, 281, 101–118. https://doi.org/10.1016/j.sedgeo.2012.08.006

Armijo, R., Meyer, B., King, G. C. P., Rigo, A., Papanastassiou, D. (1996) Quaternary evolution of the Corinth rift and its implications for the Late Cenozoic evolution of the Aegean. *Geophysical Journal International*, 126(1), 11-53. https://doi.org/10.1111/j.1365-246X.1996.tb05264.x

Armijo, R., Meyer, B., Hubert, A., Barka, A. (1999) Westward propagation of the north Anatolian into the northern Aegean: timing and kinematics. *Geology*, 27(3), 267-270. https://doi.org/10.1130/0091-7613(1999)027<0267:WPOTNA>2.3.CO;2

Arp G. (1995) Lacustrine bioherms, spring mounds, and marginal carbonates of the Ries-Impact-crater (Miocene, Southern Germany). *Facies*, 33, 35-90. https://doi.org/10.1007/BF02537444

Asaeda, T., Rajapakse, L., Sanderson, B. (2007) Morphological and reproductive acclimations to growth of two charophyte species in shallow and deep water. *Aquatic Botany*, 86(4), 393−401. https://doi.org/10.1016/j.aquabot.2007.01.010

Aschoff, J.L., Schmitt, J.G. (2008) Distinguishing Syntectonic Unconformity Types to Enhance Analysis of Growth Strata: An Example from the Cretaceous, Southeastern Nevada, U.S.A. *Journal of Sedimentary Research*, 78(9), 608-623. https://doi.org/10.2110/jsr.2008.069

Bailly, C. (2019) *Caractérisation géologique et géophysique multi-échelle des carbonates lacustres de l'île de Samos (Miocène Supérieur, Grèce) – Liens entre faciès, diagenèse et propriétés élastiques.* PhD Thesis, PSL University, Paris.

Bailly C., Adelinet M., Hamon Y., Fortin J. (2019) Combined controls of sedimentology and diagenesis on seismic properties in lacustrine and palustrine carbonates (Upper Miocene, Samos Island, Greece). *Geophysical Journal International*, 219(2), 1300–1315. https://doi.org/10.1093/gji/ggz365

Báldi, T. (1973) *Mollusc Fauna of the Hungarian Upper Oligocene (Egerian), Studies in Stratigraphy, Paleoecology, Paleogeography and Systematics.* Akadémiai Kiadó, Budapest.

Beniest, A., Brun, J.-P., Gorini, C., Crombez, V., Deschamps, R., Hamon, Y., Smit, J. (2016) Interaction between trench retreat and Anatolian escape as recorded by neogene basins in the northern Aegean Sea. *Mar. Pet. Geol.*, 77, 30-42. https://doi.org/10.1016/j.marpetgeo.2016.05.011

Böger, H., Gersonde, R., Willmann, R. (1974) Das Neogen im Osten der Insel Kos (Agäis, Dodekanes) - Stratigraphie und Tektonik. *N. Jb. Geol. Paläont. Abh.*, 145, 129-152.

Bohme, M., Van Baak, C.G.C., Prieto, J., Winklhofer, M., Spassov, N. (2018) Late Miocene stratigraphy, palaeoclimate and evolution of the Sandanski Basin (Bulgaria) and the chronology of the Pikermian faunal changes. *Glob. Planet. Change*, 170, 1–19. https://doi.org/10.1016/j.gloplacha.2018.07.019

Boronkay, K., Doutsos, T. (1994) Transpression and transtension within different structural levels in the central Aegean region. *Journal of Structural Geology*, 16, 1555–1573. https://doi.org/10.1016/0191-8141(94)90033-7

Bridge, J.S. (1993) The interaction between channel geometry, water flow, sediment transport and deposition in braided rivers. In: Best, J.L., Bristow, C.S. (Eds.), Braided Rivers. Vol. 75. Geological Society of London, pp. 13–71 Special Publication. https://doi.org/10.1144/GSL.SP.1993.075.01.02

Brun, J.P., Faccenna, C., Gueydan, F., Sokoutis, D., Philippon, M., Kydonakis, K. Gorini, C. (2016) The two-stage aegean extension, from localized to distributed, a result of slab rollback acceleration. *Canadian journal of earth sciences*, 53 (11), 1142-1157. https://doi.org/10.1139/cjes-2015-0203

Bustillo, M.A., Armenteros, I., Huerta P. (2017) Dolomitization, gypsum calcitization and silicification in carbonate–evaporite shallow lacustrine deposits. *Sedimentology*, 64(4), 1147-1172. https://doi.org/10.1111/sed.12345

Bustillo, M.A., Arribas, M.E., Bustillo, M. (2002) Dolomitization and silicification in low energy lacustrine carbonates (Paleogene, Madrid Basin, Spain). *Sedimentary Geology*, 151, 107–126. https://doi.org/10.1016/S0037-0738(01)00234-2

Butiseacă, G.A., Vasiliev, I., van der Meer, M.T.J., Krijgsman, W., Palcu, D.V., Feurdean, A., Niedermeyer, E.M., Mulch, A. (2021) Severe late Miocene droughts affected western Eurasia. *Global and Planetary Change*, 206, 103644. https://doi.org/10.1016/j.gloplacha.2021.103644

Camoin G., Casanova J., Rouchy J.-M., Blanc-Valleron M.-M., Deconinck J.-F. (1997) Environmental controls on perennial and ephemeral carbonate lakes: the central palaeo-Andean Basin of Bolivia during Late Cretaceous to early Tertiary times. *Sedimentary Geology*, 113, 1-26. https://doi.org/10.1016/S0037-0738(97)00052-3

Carlsson, R. (2006) Freshwater snail assemblages of semi-isolated brackish water bays on the Åland Islands, SW Finland. *Boreal Environment Research*, 11, 371-382.

Casagranda, C., Boudouresque, C., Francour, F., Abundance P; (2005) Population structure and Production of *Hydrobia ventrosa* (Gastropoda: Prosobranchia) in a Mediterranean brackish lagoon, Lake Ichkeul, Tunisia. *Archiv fur Hydrobiologie*, 164(3), 411-428. https://doi.org/10.1127/0003-9136/2005/0164-0411

Castle J. (1991) Sedimentation in Eocene Lake Uinta (Lower Green River Formation), Northwestern Uinta Basin, Utah. In: Katz B.J. (Ed.) *Lacustrine Basin Exploration-Case Studies and Modern Analogs.* AAPG Memoir, 50, 243-264. https://doi.org/10.1306/M50523C15

Chanvry, E., Deschamps, R., Joseph, P., Puigdefàbregas, C., Poyatos-Moré, M., Serra-Kiel, J., Garcia, D., Teinturier, S. (2018) The influence of intrabasinal tectonics in the stratigraphic evolution of piggyback basin fills: Towards a model from the Tremp-Graus-Ainsa Basin (South-Pyrenean Zone, Spain). *Sedimentary Geology*, 377, 34–62. https://doi.org/10.1016/j.sedgeo.2018.09.007

Clausing A. (1990) Mikrofazies lakustrine Karbonat-horizonte des Saar-Nahe-Beckens (Unterperm, Rotliegend, SW-Deutschland). *Facies*, 23, 121-140. https://doi.org/10.1007/BF02536710

Cole, R.B., DeCelles, P.G. (1991) Subaerial to submarine transitions in early Miocene pyroclastic flow deposits, southern San Joaquin basin, California. *Bull. geol. Soc. Am.*, 103, 221-235. https://doi.org/10.1130/0016-7606(1991)103<0221:STSTIE>2.3.CO;2

Collinson, M.E. (2002) The ecology of Cainozoic ferns. *Review of Palaeobotany and Palynology*, 119, 51–68. https://doi.org/10.1016/S0034-6667(01)00129-4

Dean, W.E., Fouch, T.D. (1983) Lacustrine Environment (Chapter 2). In: Scholle, P.A., Bebout, D.G., Moore, C.H. (Eds.) *Carbonate Depositional Environments.* AAPG Memoir, 33, 97-116. https://doi.org/10.1306/M33429C6

DeCelles, P.G., Gray, M.B., Ridgway, K.D., Cole, R.B., Pivnik, D.A., Pequera, N., Srivastava, P. (1991) Controls on synorogenic alluvial-fan architecture, Beartooth Conglomerate (Paleocene), Wyoming and Montana. *Sedimentology*, 38, 567-590. https://doi.org/10.1111/j.1365-3091.1991.tb01009.x

Dickson, J.A.D. (1966) Carbonate identification and genesis as revealed by staining. *Journal of Sedimentary Research*, 36(2), 491-505. https://doi.org/10.1306/74D714F6-2B21-11D7-8648000102C1865D

Dunagan, S.P., Turner, C.E. (2004) Regional paleohydrologic and paleoclimatic settings of wetland/lacustrine depositional systems in the Morrison Formation (Upper Jurassic), Western Interior, USA. *Sedimentary Geology*, 167, 269–296. https://doi.org/10.1016/j.sedgeo.2004.01.007

Enos, P. (1977) Flow regimes in debris flow. *Sedimentology*, 24, 133-142. https://doi.org/10.1111/j.1365-3091.1977.tb00123.x

Eronen, J.T. (2006) Eurasian Neogene large herbivorous mammals and climate. *Acta Zoologica Fennica*, 216, 1–72. http://urn.fi/URN:ISBN:951-9481-63-X

Eronen, J., Ataabadi, M.M., Micheels, A., Karme, A., Bernor, R. L., Fortelius, M. (2009) Distribution history and climatic controls of the Late Miocene Pikermian chronofauna. *PNAS*, 106(29), 11867–11871. https://doi.org/10.1073/pnas.0902598106

Ferentinos, G., Georgiou, N., Christodoulou, D., Geraga, M., Papatheodorou, G. (2018) Propagation and termination of a strike slip fault in an extensional domain: The westward growth of the North Anatolian Fault into the Aegean Sea. *Tectonophysics*, 745, 183-195. https://doi.org/10.1016/j.tecto.2018.08.003

Finkelstein, D.B., Hay, R.L., Altaner, S.P. (1999) Origin and diagenesis of lacustrine sediments, upper Oligocene Creede Formation, southwestern Colorado. *Geological Society of America Bulletin*, 111, 1175–1191. https://doi.org/10.1130/0016-7606(1999)111<1175:OADOLS>2.3.CO;2

Flecker, R., Krijgsman, W., Capella, W., de Castro Martíns, C., Dmitrieva, E., Mayser, J.P., Marzocchi, A., Modestu, S., Ochoa, D., Simon, D., Tulbure, M., van den Berg, B., van der Schee, M., de Lange, G., Ellam, R., Govers, R., Gutjahr, M., Hilgen, F., Kouwenhoven, T., Lofi, J., Meijer, P., Sierro, F.J., Bachiri, N., Barhoun, N., Alami, A.C., Chacon, B., Flores, J.A., Gregory, J., Howard, J., Lunt, D., Ochoa, M., Pancost, R., Vincent, S., Yousfi, M.Z. (2015) Evolution of the Late Miocene Mediterranean-Atlantic gateways and their impact on regional and global environmental change. *Earth-Science Reviews*, 150, 365–392. https://doi.org/10.1016/j.earscirev.2015.08.007

Ford, T.D., Pedley, M. (1996) A review of the tufa and travertine deposits of the World. *Earth-Science Reviews*, 41, 117-175. https://doi.org/10.1016/S0012-8252(96)00030-X

Fortelius, M., Eronen, J., Liu, L., Pushkina, D., Tesakov, A., Vislobokova, I., Zhang, Z. (2006) Late Miocene and Pliocene large land mammals and climatic changes in Eurasia. *Palaeogeography, Palaeoclimatology, Palaeoecology*, 238(1–4), 219-227. https://doi.org/10.1016/j.palaeo.2006.03.042

Freytet, P. (1973) Petrography and paleo-environement of continental carbonate deposits with particular reference to the upper cretaceous and lower Eocene of Languedoc (Southern France). *Sedimentary Geology*, 10 (1), 25–60. https://doi.org/10.1016/0037-0738(73)90009-2

Freytet, P., Verrecchia, E.P. (2002) Lacustrine and palustrine carbonate petrography: an overview. *Journal of Paleolimnology*, 27, 221–237. https://doi.org/10.1023/A:1014263722766

Gasse F., Fontes, J. C., Plaziat, J. C., Carbonel, P., Kaczmarska, I., De Deckker, P., Soulie-Marsche, I., Callot, I., Dupeuble, P.A. (1987) Biological remains, geochemistry and stable isotopes for the reconstruction of environmental and hydrological changes in the Holocene lakes from North Sahara. *Palaeogeogr. Palaeoclimatol. Palaeoecol.*, 60, 1–46. https://doi.org/10.1016/0031-0182(87)90022-8

Gessner, K., Gallardo, L.A., Markwitz, V., Ring, U., Thomson, S.N. (2013) What caused the denudation of the Menderes Massif: Review of crustal evolution, lithosphere structure, and dynamic topography in southwest Turkey. *Gondwana Research*, 24(1), 243-274. https://doi.org/10.1016/j.gr.2013.01.005

Giaourtsakis, I.X., Koufos, G.D. (2009) The Late Miocene Mammal Faunas of the Mytilinii Basin, Samos Island, Greece: New Collection - 10. Chalicotheriidae. *Beitr. Paläont.*, 31, 189–205

Gierlowski-Kordesch, E.H. (2010) Lacustrine Carbonates (Chapter 1). In: Alonso-Zarza A.M., Tanner L. H. (Eds.) *Carbonates in continental settings: Facies, Environments, and Processes.* Developments in sedimentology, 61, Elsevier, 1-101. https://doi.org/10.1016/S0070-4571(09)06101-9

Göktaş, F. (2014) Neogene Stratigraphy and paleogegraphic evolution of the Karaburun Peninsula, Izmir, Western Turkey. *Bulletin of the Mineral Research and Exploration*, 149, 69-92.

Göktaş, F. (2020) Neogene stratigraphy and regional correlation of the Çeşme Peninsula, Western Anatolia, Turkey. *Bulletin of the Mineral Research and Exploration*, 162, 31-54.

Haq, B.U., Hardenbol, J., Vail, P.R. (1987) Chronology of fluctuating sea levels since the Triassic. *Science*, 235, 1156–1167. http://doi.org/10.1126/science.235.4793.1156

Hamon, Y., Deschamps, R., Bailly, C., Adelinet, M., Gorini, C. (2017) Characterization of the lacustrine series of Miocene age as markers for climatic and tectonic regional evolution of the East Aegean region. *33rd IAS & 16th ASF Joint Meeting*. Toulouse, France.

Helvaci, C., Stamatakis, M.G., Zagouroglou, C, Kanaris, J. (1993) Borate Minerals and Related Authigenic Silicates in Northeastern Mediterranean Late Miocene Continental Basins. *Explor. Mining Geol.*, 2(2), 171-178.

Hilgen, F.J., Lourens, L.J., Van Dam, J.A. (2012) Chapter 29 - The Neogene Period. In: Gradstein, F.M., Ogg, J.G., Schmitz, M.D., Ogg, G.M. (Eds.) *The Geological Time Scale 2012*. Elsevier B.V., Amsterdam, 947–1002. https://doi.org/10.1016/B978-0-444-59425-9.00029-9

Hillaire-Marcel C., Casanova J. (1987) Isotopic hydrology and paleohydrology of the Magadi (Kenya) - Natron (Tanzania) basin during the late Quaternary. *Palaeogeography, Palaeoclimatology, Palaeoecology*, 58, 155-181. https://doi.org/10.1016/0031-0182(87)90058-7

Hofmann, A.M., Geist, J., Nowotny, L., Raeder, U. (2020) Depth-distribution of lake benthic diatom assemblages in relation to light availability and substrate: implications for paleolimnological studies. *Journal of Paleolimnology*, 64, 315–334. https://doi.org/10.1007/s10933-020-00139-9

Horton, B.K., Schmitt, J.G. (1996) Sedimentology of a lacustrine fan-delta system, Miocene Horse Camp Formation, Nevada, USA. *Sedimentology*, 43, 133-155. https://doi.org/10.1111/j.1365-3091.1996.tb01464.x

Huerta, P., Armenteros, I. (2005) Calcrete and palustrine assemblages on a distal alluvial-floodplain: a response to local subsidence (Miocene of the Duero basin, Spain). *Sedimentary Geology*, 177, 253–270. https://doi.org/10.1016/j.sedgeo.2005.03.007

Ioakim, C., Koufos, G.D. (2009) The Late Miocene Mammal Faunas of the Mytilinii Basin, Samos Island, Greece: New Collection - 3. Palynology. *Beitr. Paläont.*, 31, 27–35.

Ioakim C., Rondoyanni, T., Mettos, A. (2005) The Miocene Basins of Greece (Eastern Mediterranean) from a palaeoclimatic perspective. *Revue de Paléobiologie*, 24 (2), 735-748.

Ioakim, C., Solounias, N. (1985) A radiometrically dated pollen flora from the Upper Miocene of Samos Island, Greece. *Revue de Micropaléontologie*, 28(3), 197-204.

John, J. (2020) *Diatoms from arid Australia: taxonomy and biogeography.* The diatom flora of Australia, 3, Schmitten – Oberreifenberg.

Jolivet, L., Brun, J. P., Gautier, P., Lallemant, S., Patriat, M. (1994) 3D-kinematics of extension in the Aegean region from the early Miocene to the present, insights from the ductile crust. *Bulletin de la Société Géologique de France*, 165(3), 195-209.

Jolivet, L., Faccenna, C., Huet, B., Labrousse, L., Le Pourhiet, L., Lacombe, O., Lecomte, E., Burov, E., Denèle, Y., Brun, J.-P. (2013) Aegean tectonics: strain localisation, slab tearing and trench retreat. *Tectonophysics*, 597, 1–33. https://doi.org/10.1016/j.tecto.2012.06.011

Jolivet, L., Menant, A., Sternai, P., Rabillard, A., Arbaret, L., Augier, R., Laurent, V., Beaudoin, A., Grasemann, B., Huet, B., Labrousse, L., Le Pourhiet, L. (2015) The geological signature of a slab tear below the Aegean. *Tectonophysics*, 659, 166-182. https://doi.org/10.1016/j.tecto.2015.08.004

Juřičková L., Horsák M., Beran, L. (2001) Check-list of the molluscs (Mollusca) of the Czech Republic. *Acta Soc. Zool. Bohem.*, 65, 25-40.

Kantiranis, N., Filippidis, A., Stamatakis, M., Tzamos, E., Drakoulis, A. (2007) A preliminary study of the colemanite-rich tuff layer from the Sourides area, Karlovassi Basin, Samos Island, Hellas. *Bulletin of the Geological Society of Greece*, 40(2), 769-774. https://doi.org/10.12681/bgsg.16717

Kaya, O., Ünay, E., Saraç, G., Eichhorn, S., Hassenrück, S., Knappe, A., Pekdeğer, A., Mayda, S. (2004) Halitpafla Transpressive Zone: Implications for an Early Pliocene compressional phase in Central Western Anatolia, Turkey. *Turkish Journal of Earth Sciences*, 13, 1-13.

Keighley, D. (2008) A lacustrine shoreface succession in the Albert Formation, Moncton Basin, New Brunswick. *Bulletin of Canadian Petroleum Geology*, 56(4), 235-258. https://doi.org/10.2113/gscpgbull.56.4.235

Kissel, C., Laj, C. (1988) The tertiary geodynamic evolution of the Aegean arc: a paleomagnetic reconstruction. *Tectonophysics*, 146, 183–201. https://doi.org/10.1016/0040-1951(88)90090-X

Klappa, C. (1980) Rhizoliths in terrestrial carbonates: classification, recognition, genesis and significance. *Sedimentology*, 27, 613–629. https://doi.org/10.1111/j.1365-3091.1980.tb01651.x

Kociolek, J.P., Khursevich, G.K. (2013) Morphology of some fossil lacustrine centric species from the western United States assigned to the genus *Cyclotella* (*Bacillariophyta*), including four described as new. *Phytotaxa*, 127, 81-99. https://doi.org/10.11646/phytotaxa.127.1.11

Kostopoulos, D.S. (2009a) The Late Miocene Mammal Faunas of the Mytilinii Basin, Samos Island, Greece: New Collection - 13. Giraffidae. *Beitr. Paläont.*, 31, 299–343.

Kostopoulos, D.S. (2009b) The Late Miocene Mammal Faunas of the Mytilinii Basin, Samos Island, Greece: New Collection – 14. Bovidae. *Beitr. Paläont.*, 31, 345–389.

Kostopoulos, S.D., Sen, S., Koufos, D.G. (2003) Magnetostratigraphy and revised chronology of the late Miocene mammal localities of Samos, Greece. *International Journal of Earth Sciences*, 92, 779-794. https://doi.org/10.1007/s00531-003-0353-8

Koufos, G.D. (2006) The Neogene mammal localities of Greece: Faunas, chronology and biostratigraphy. *Hellenic Journal of Geosciences*, 41, 183-214.

Koufos, G.D., Kostopoulos, D.S., Vlachou, T.D., Konidaris, G.E. (2011) A synopsis of the late Miocene Mammal Fauna of Samos Island, Aegean Sea, Greece. *Geobios*, 44, 237–251. https://doi.org/10.1016/j.geobios.2010.08.004

Koufos, G.D., Syrides, G.E., Kostopoulos, D.S., Koliadimou, K.K., Sylvestrou, I.A., Seitanidis, G.Ch., Vlachou, T.D. (1997) New excavations in the Neogene mammalian localities of Mytilinii, Samos Island, Greece. *Geodiversitas*, 19(4), 877-885.

Krijgsman, W., Palcu, D.V., Andreetto, F., Stoica, M., Mandic, O. (2020) Changing seas in the late Miocene Northern Aegean: A Paratethyan approach to Mediterranean basin evolution. *Earth-Science Reviews*, 210, 103386. https://doi.org/10.1016/j.earscirev.2020.103386.

Krijgsman, W., Stoica, M., Vasiliev, I., Popov, V. V. (2010) Rise and fall of the Paratethys Sea during the Messinian Salinity Crisis. *Earth and Planetary Science Letters*, 290, 183–191. https://doi.org/10.1016/j.epsl.2009.12.020

Lazzarini, L., Cancelliere, S. (2000) Characterisation of the white marble of two unpublished ancient Roman quarries on the Islands of Fourni and Skyros (Greece). *Per. Mineral.*, 69(1), 49-62.

Le Pichon, X., Angelier, J. (1981) The Aegean Sea [and Discussion]. *Philosophical Transactions of The Royal Society of London. Series A, Mathematical Physical and Engineering Sciences*, 300(1454), 357-372. https://doi.org/10.1098/rsta.1981.0069

Leier, A.L., DeCelles, P.G., Pelletier, J.D. (2005) Mountains, monsoons, and megafans: *Geology*, 33, 289-292, https://doi.org/10.1130/G21228.1

Lettéron, A., Fournier, F., Hamon Y., Villier, L., Margerel, J.-P., Bouche, A., Feist, M., Joseph, P. (2017) Multi-proxy paleoenvironmental reconstruction of saline lake carbonates: paleoclimatic and paleogeographic implications (Priabonian-Rupelian, Issirac Basin, SE France). *Sedimentary Geology*, 358, 97-120. https://doi.org/10.1016/j.sedgeo.2017.07.006

Lettéron, A., Hamon Y., Fournier, F., Séranne, M., Pellenard, P. Joseph, P. (2018) Reconstruction of a saline, lacustrine carbonate system (Priabonian, St-Chaptes Basin, SE France): depositional models, paleogeographic and paleoclimatic implications. *Sedimentary Geology*, 367, pp.20-47. https://doi.org/10.1016/j.sedgeo.2017.12.023

Ligios, S., Anadón P., Castorina, F., D'Amico C., Esu D., Gliozzi, E., Gramigna, P., Mola, M., Monegato, G. (2012) Ostracoda and Mollusca biodiversity and hydrochemical features in Late Miocene brackish basins of Italy. *Geobios*, 45, 351–367. https://doi.org/10.1016/j.geobios.2011.10.008

Lindqvist, J.K., Lee, D.E. (2009) High-frequency paleoclimate signals from Foulden Maar, Waipiata Volcanic Field, southern New Zealand: An Early Miocene varved lacustrine diatomite deposit. *Sedimentary Geology*, 222(1–2), 98-110. https://doi.org/10.1016/j.sedgeo.2009.07.009

Lokier, S.W., Al Junaibi M. (2016) The petrographic description of carbonate facies: are we all speaking the same language? *Sedimentology*, 63, 1843-1885. https://doi.org/10.1111/sed.12293

Lowe, D.R. (1979) Sediment gravity flows: their classification and some problems of application to natural flows and deposits. In: Doyle, L.J., Pilkey, O.H. (Eds.) *Geology of Continental Slopes*. Society of Economic Paleontologists and Mineralogists, Special Publication 27, p. 75-82. https://doi.org/10.2110/pec.79.27.0075

Löwen, K., Bröcker, M., Berndt, J. (2015) Depositional ages of clastic metasediments from Samos and Syros, Greece: results of a detrital zircon study. *Int. J. Earth Sci. (Geol. Rundsch.)*, 104, 205-220. https://doi.org/10.1007/s00531-014-1058-x

McArthur J.M., Howarth, R.J. (2004) Strontium Isotope Stratigraphy. In: Gradstein, F., Ogg, J., Smith, A. (Eds.) *A Geological Timescale*, Cambridge University Press, pp.96-105. https://doi.org/10.1016/B978-0-444-59425-9.00007-X

McKenzie, J.A. (1985) Carbon isotopes and productivity in the lacustrine and marine environment. In: Stumm W. (Ed.) *Chemical Processes in Lakes*. Wiley, 99-118.

Mees, F., Casteñeda, C., Herrero, J., Van Ranst, E. (2012) The nature and significance of variations in gypsum crystal morphology in dry lake basins. *Journal of Sedimentary Research*, 82, 37–52. https://doi.org/10.2110/jsr.2012.3

Meissner, B. (1976) Das Neogen von Ost-Samos. Sedimentations-geschichte und Korrelation. *Neues Jahrbuch für Geologie und Paläontologie Abhandlung*, B152(2), 161-176.

Menant, A., Jolivet, L., Augier, R., Skarpelis, N. (2013) The North Cycladic Detachment System and associated mineralization, Mykonos, Greece: insights on the evolution of the Aegean domain. *Tectonics*, 32, 433–452. https://doi.org/10.1002/tect.20037

Meulenkamp, J. (1971) The Neogene in the southern Aegean area. Opera Bot., 30, 5–12.

Mezger, K., Altherr, R., Okrusch, M., Henjes-Kunst, F., Kreuzer H. (1985) Genesis of acid/basic rock associations: a case study The Kallithea intrusive complex, Samos, Greece. *Contrib. Mineral. Petrol.*, 90, 353-366.

Miall, A.D. (1977) A review of the braided river depositional environment. *Earth Science Reviews*, 13, p. 1-62. https://doi.org/10.1016/0012-8252(77)90055-1

Miall, A.D. (1996) *The geology of fluvial deposits. Sedimentary facies, Basin analysis, and petroleum Geology*. Springer, Berlin. https://doi.org/10.1007/978-3-662-03237-4

Nemec, W., Steel, R.J. (1984) Alluvial and coastal conglomerates: their significant features and some comments on gravelly mass-flow deposits. In: Koster, E.H., Steel R.J. (Eds.) *Sedimentology of Gravels and Conglomerates*, Mem. Can. Soc. petrol. Geol., 10, 1-31.

Ocakoğlu, N., Demirbağ, E., Kuşçu, I. (2004) Neotectonic structures in the area offshore of Alaçatı, Doğanbey and Kuşadası (western Turkey): evidence of strike-slip faulting in the Aegean extensional province. *Tectonophysics*, 391(1–4), 67-83. https://doi.org/10.1016/j.tecto.2004.07.008

Ocakoğlu, N., Demirbağ, E., Kuşçu, I. (2005) Neotectonic structures in İzmir Gulf and surrounding regions (western Turkey): Evidences of strike-slip faulting with compression in the Aegean extensional regime, *Marine Geology*, 219(2–3), 155-171. https://doi.org/10.1016/j.margeo.2005.06.004

Ordóñez, S, García-Del-Cura, M.A. (1983) Recent and Tertiary fluvial carbonates in central Spain. In: Collinson, J.D., Lewin, J. (Eds.) *Ancient and Modern Fluvial System*, IAS Special Publication, 6, 485-497. https://doi.org/10.1002/9781444303773.ch39

Owen, R. B., Crossley R. (1992) Spatial and temporal distribution of diatoms in sediments of Lake Malawi, Central Africa, and ecological implications. *Journal of Paleolimnology*, 7, 55–71. https://doi.org/10.1007/BF00197031

Owen, R.B., Renaut, R.W., Stamatakis, M.G. (2011) Late Miocene lacustrine sedimentation in the Mytilinii Basin, Samos Island, Greece. *J. Paleolimnol.*, 46, 151-166. https://doi.org/10.1007/s10933-011-9530-0

Palcu, D.V., Patina, I.S., Şandric, I., Lazarev S., Vassiliev I., Stoica M., Krijgsman W. (2021) Late Miocene megalake regressions in Eurasia. *Sci. Rep.*, 11, 11471. https://doi.org/10.1038/s41598-021-91001-z

Palcu, D.V., Vasiliev, I., Stoica, M., Krijgsman, W. (2019) The end of the Great Khersonian Drying of Eurasia: Magnetostratigraphic dating of the Maeotian transgression in the Eastern Paratethys. *Basin Research*, 31(1), 33-58. https://doi.org/10.1111/bre.12307

Pe-Piper, G., Piper, D.J.W. (2007) Late Miocene igneous rocks of Samos: the role of tectonism in petrogenesis in the southeastern Aegean. In: Taymaz, T., Yilmaz, Y., Dilek, Y. (Eds.) *The Geodynamics of the Aegean and Anatolia.* Geological Society of London, Special Publications, 291, 75–97. https://doi.org/10.1144/SP291.4

Pedley, H.M. (1990) Classification and environmental models of cool freshwater tufas. *Sedimentary Geology*, 68, 143-154. https://doi.org/10.1016/0037-0738(90)90124-C

Pedley, M. (2009) Tufas and travertines of the Mediterranean region: A testing ground for freshwater carbonate concepts and developments. *Sedimentology*, 56(1), 221-246. https://doi.org/10.1111/j.1365-3091.2008.01012.x

Pellegrino, L., Dela Pierre, F., Natalicchio, M., Carnevale, G. (2018) The Messinian diatomite deposition in the Mediterranean region and its relationships to the global silica cycle. *Earth-Science Reviews*, 178, 154-176. https://doi.org/10.1016/j.earscirev.2018.01.018

Platt, N.H., Wright, V.P. (1991) Lacustrine carbonates: facies models, facies distributions and hydrocarbon aspects. In: Anadon P., Cabrera L, Kelts K. (eds) *Lacustrine facies analysis.* IAS Spec. Pub., 13, 57-74. https://doi.org/10.1002/9781444303919.ch3

Popov, S.V., Antipov, M.P., Zastrozhnov, A.S., Kurina, E.E., Pinchuk, T.N. (2010) Sea-level fluctuations on the northern shelf of the Eastern Paratethys in the Oligocene-Neogene. *Stratigr. Geol. Correl.*, 18, 200–224. https://doi.org/10.1134/S0869593810020073

Reineck, H.E., Singh, I.B. (1980) *Depositional Sedimentary Environments. With reference to terrigenous clastics.* Springer-Verlag, New York. https://doi.org/10.1007/978-3-642-81498-3

Rhodes, M. K., Carroll, A. R., Pietras, J. T., Beard, B. L., Johnson, C. M. (2002) Strontium isotope record of paleohydrology and continental weathering, Eocene Green River Formation, Wyoming. *Geology*, 30(2), 167–170. https://doi.org/10.1130/0091-7613(2002)030<0167:SIROPA>2.0.CO;2

Riding, R. (1979) Origin and diagenesis of lacustrine algal bioherms at the margin of the Ries crater, Upper Miocene, southern Germany. *Sedimentology*, 26, 645-680. https://doi.org/10.1111/j.1365-3091.1979.tb00936.x

Ring, U., Laws, S., Bernet, M. (1999) Structural analysis of a complex nappe sequence and late-orogenic basins from the Aegean Island of Samos, Greece. *J. Struct. Geol.*, 21, 1575–1601. https://doi.org/10.1016/S0191-8141(99)00108-X

Ring, U., Okrusch, M., Will, T. (2007) Samos Island, part I: metamorphosed and non-metamorphosed nappes, and sedimentary basins. *J. Virt. Explor.*, 27, 1-28 (Paper 5). https://doi.org/10.3809/jvirtex.2007.00180

Ring, U., Gessner, K., Thomson, S. (2017) Variations in fault-slip data and cooling history reveal corridor of heterogeneous backarc extension in the eastern Aegean Sea region. *Tectonophysics*, 700–701, 108–130. https://doi.org/10.1016/j.tecto.2017.02.013

Roche, A., Vennin, E., Bouton, A., Olivier, N., Wattinne, A., Bundeleva, I., Deconinck, J.F., Virgone A., Gaucher, E., Visscher P. (2018) Oligo-Miocene lacustrine microbial and metazoan buildups from the Limagne Basin (French Massif Central). *Palaeogeography, Palaeoclimatology, Palaeoecology*, 504, 34-59. https://doi.org/10.1016/j.palaeo.2018.05.001

Roche V., Jolivet L., Papanikolaoue, D., Bozkurt E., Menant A., Rimmelé G. (2019) Slab fragmentation beneath the Aegean/Anatolia transition zone: Insights from the tectonic and metamorphic evolution of the Eastern Aegean region. *Tectonophysics*, 754, 101–129. https://doi.org/10.1016/j.tecto.2019.01.016

Rodriguez-Pascua, M.A., Calvo, J.P., De Vicente, G., Gomez-Gras, D. (2000) Soft-sediment deformation structures interpreted as seismites in lacustrine sediments of the Prebetic Zone, SE Spain, and their potential use as indicators of earthquake magnitudes during the Late Miocene. *Sedimentary Geology*, 135, 117-135. https://doi.org/10.1016/S0037-0738(00)00067-1

Rosenbaum, J., Sheppard, S. M. (1986) An isotopic study of siderites, dolomites and ankerites at high temperatures. *Geochim. Cosmochim. Acta*, 50, 1147-1150. https://doi.org/10.1016/0016-7037(86)90396-0

Roveri, M., Flecker, R., Krijgsman, W., Lofi, J., Lugli, S., Manzi, V., Sierro, F.J., Bertini, A., Camerlenghi, A., De Lange, G., Govers, R., Hilgen, F.J., Hübscher, C., Meijer, P.T., Stoica, M. (2014) The Messinian Salinity Crisis: past and future of a great challenge for marine sciences. *Marine Geology*, 352, 25–58. https://doi.org/10.1016/j.margeo.2014.02.002

Rust, B.R. (1978) Depositional models for braided alluvium. In: Miall, A.D. (Ed.) *Fluvial Sedimentology*. Canadian Society of Petroleum Geologists, Memoir 5, 605-625.

Sáez, A., Cabrera, L. (2002) Sedimentological and palaeohydrological responses to tectonics and climate in a small, closed, lacustrine system: Oligocene As Pontes Basin (Spain). *Sedimentology*, 49, 1073–1094. https://doi.org/10.1046/j.1365-3091.2002.00490.x

Sakellariou, D., Tsampouraki-Kraounaki, K. (2019) Plio-Quaternary extension and strike-slip tectonics in the Aegean. In: Duarte J. (Ed.) *Transform Plate Boundaries and Fracture Zones, Chapter 14*. Elsevier, p. 339-374. https://doi.org/10.1016/B978-0-12-812064-4.00014-1

Sakınç, M., Yaltırak, C. (2005) Messinian crisis: What happened around the northeastern Aegean? *Marine Geology*, 221(1–4), 423-436. https://doi.org/10.1016/j.margeo.2005.03.018.

Sakınç, M., Yaltırak, C., Oktay, F.Y. (1999) Palaeogeographical evolution of the Thrace Neogene Basin and the Tethys–Paratethys relations at northwestern Turkey (Thrace). *Palaeogeography, Palaeoclimatology, Palaeoecology*, 153(1–4), 17-40. https://doi.org/10.1016/S0031-0182(99)00071-1

Sasaki, H., Sasaki, Y., Saito-Kato, M., Naruse, H., Ishihara, Y. (2020) Bed-thickness frequency distributions and recurrence intervals of sediment-gravity-flow deposits intercalated in lacustrine varved diatomite: examples from the middle Pleistocene Hiruzenbara Formation, southwest Japan. *Journal of Sedimentary Research*, 90 (6), 561–572. https://doi.org/10.2110/jsr.2020.28

Schmitz, B., Pujalte, V. (2007) Abrupt increase in seasonal extreme precipitation at the Paleocene-Eocene boundary. *Geology*, 35(3), 215–218; https://10.1130/G23261A.1

Sen, S., Valet, J.-P. (1986) Magnetostratigraphy of late Miocene continental deposits in Samos, Greece. *Earth and Planetary Science Letters*, 80, 167–174. http://dx.doi.org/10.1016/0012-821x(86)90030-0

Smith, G.A. (1986) Coarse-grained nonmarine volcaniclastic sediment: terminology and depositional process. *Bull. geol. Soc. Am.*, 97, 1-10. https://doi.org/10.1130/0016-7606(1986)97%3c1:CNVSTA%3e2.0.CO;2

Smith, S.A. (1990) The sedimentology and accretionary styles of an ancient gravel-bed stream; the Budleigh Salterton pebble beds (Lower Triassic), Southwest England. *Sedimentary Geology*, 67(3-4), 199-219. https://doi.org/10.1016/0037-0738(90)90035-R

Smith, N.D., Cross, T.A., Dufficy, J.P., Clough, S.R. (1989) Anatomy of an avulsion. *Sedimentology*, 36, 1–23. https://doi.org/10.1111/j.1365-3091.1989.tb00817.x

Sohn, Y.K., Rhee, C.W., Kim, B.C. (1999) Debris flow and hyperconcentrated flood-flow deposits in an alluvial fan, northwestern part of the Cretaceous Yongdong basin, Central Korea. *Journal of Geology*, 107, 111-132. https://doi.org/10.1086/314334

Stamatakis, M.G., Economou, S.G. (1991) A colemanite and ulexite occurrence in a Late Miocene saline-alkaline lake of West Samos Island, Greece. *Economic Geology*, 86/1, 166-172. https://doi.org/10.2113/gsecongeo.86.1.166

Stamatakis, M.G., Hein, J., Magganas, A. (1989) Geochemistry and diagenesis of Miocene lacustrine siliceous sedimentary and pyroclastic rocks, Mytilinii basin, Samos Island, Greece. *Sedimentary Geology*, 64, 65-78. https://doi.org/10.1016/0037-0738(89)90084-5

Stamatakis, M.G., Tziritis, E.P., Evelpidou N. (2009) The geochemistry of Boron-rich groundwater of the Karlovassi Basin, Samos Island, Greece. *Open Geosciences*, 1(2), 207-218. https://doi.org/10.2478/v10085-009-0017-4

Steininger, F. F., Rögl, F. (1984) Paleogeography and palinspastic reconstruction of the Neogene of the Mediterranean and Paratethys. In: Dixon, J.E. and Robertson A.H.F. (Eds.) *The Geological Evolution of the Eastern Mediterranean.* Geol. Soc. Lond. Spec. Publ., 17, 659–668.

Talbot, M.R. (1990) A review of the palaeohydrological interpretation of carbon and oxygen isotopic ratios in primary lacustrine carbonates. *Chemical Geology*, 80, 261-279. https://doi.org/10.1016/0168-9622(90)90009-2

Talbot, M.R., Allen, P.A. (1996) Lakes. In: Reading, H.G. (Ed.). Sedimentary Environments: Processes, Facies and Stratigraphy. Blackwell Science, Oxford, 83–124.

Tari, G., Fallah, M., Schell, C., Kosi, W., Bati, Z., Sipahioğlu, N.Ö., Krezsek, C., Schleder, Z., Kozhuharov, E., Kitchka, A. (2016) Why are there no Messinian evaporites in the Black Sea? *Petroleum Geoscience*, 22(4), 381-391. https://doi.org/10.1144/petgeo2016-003

Taymaz, T., Yilmaz, Y., Dilek, Y. (2007) The Geodynamics of the Aegean and Anatolia: Introduction. In: Taymaz, T., Yilmaz, Y., Dilek, Y. (Eds.) *The Geodynamics of the Aegean and Anatolia.* Geological Society of London Special Publications, 291(1), 1-16. https://doi.org/10.1144/SP291.1

Theodoropoulos, D. (1979) Geological map of Greece – Samos Island. Institute of Geological and Mining Research. Publication Department of Geological Maps, Athens.

Trobajo, R., Cox, E.J., Quintana, X.D. (2004) The effects of some environmental variables on the morphology of Nitzschia frustulum (Bacillariophyta), in relation its use as a bioindicator. *Nova Hedwigia*, 79(3-4), 433-445. https://doi.org/10.1127/0029-5035/2004/0079-0433

Tsampouraki-Kraounaki, K., Sakellariou, D., Rousakis, G., Morfis, I., Panagiotopoulos, I., Livanos, I., Manta, K., Paraschos, F., Papatheodorou, G. (2021) The Santorini-Amorgos Shear Zone: Evidence for Dextral Transtension in the South Aegean Back-Arc Region, Greece. *Geosciences*, 11, 216 https://doi.org/10.3390/ geosciences11050216

Tzanova, A., Herbert, T.D., Peterson, L. (2015) Cooling Mediterranean Sea surface temperatures during the late Miocene provide a climate context for evolutionary transitions in Africa and Eurasia. *Earth Planet. Sci. Lett.*, 419, 71–80. https://doi.org/10.1016/j.epsl.2015.03.016

Utrilla, R., Vázquez, A., Anadón, P. (1998) Paleohydrology of the Upper Miocene Bicorb Lake (eastern Spain) as inferred from stable isotopic data from inorganic carbonates. *Sedimentary Geology*, 121, 191–206. https://doi.org/10.1016/S0037-0738(98)00086-4

van Hinsbergen, D.J.J. (2010) A key extensional metamorphic complex reviewed and restored: the Menderes massif of western Turkey. *Earth Sci. Rev.*, 102, 60-76. https://doi.org/10.1016/j.earscirev.2010.05.005

van Hinsbergen, D.J.J., Schmid S.M. (2012) Map view restoration of Aegean–West Anatolian accretion and extension since the Eocene, *Tectonics*, 31, TC5005, pp.1-40. https://doi.org/10.1029/2012TC003132

Vázquez-Urbez, M., Arenas C., Pardo, G. (2012) A sedimentary facies model for stepped, fluvial tufa systems in the Iberian Range (Spain): the Quaternary Piedra and Mesa valleys. *Sedimentology*, 59, 502-526. https://doi.org/10.1111/j.1365-3091.2011.01262.x

Wattine, A., Vennin, E., De Wever, P. (2003) Evolution d'un environnement carbonaté lacustre à stromatolithes, par l'approche paléo-écologique (carrière de Montaigu-le-Blin, bassin des Limagnes, Allier, France). *Bulletin de la Société Géologique de France*, 174, 243–260. https://doi.org/10.2113/174.3.243

Weidmann, M., Solounias, N., Drake, R.E., Curtis J. (1984) Neogene stratigraphy of the Mytilini Basin, Samos Island, Greece. *Geobios*, 17, 477-490.

Williams, P.F., Rust, B.R. (1969) The sedimentology of a braided river. *Journal of Sedimentary Research*, 39, 649–679. https://doi.org/10.1306/74D71CF3-2B21-11D7-8648000102C1865D

Willmann, R. (1981) Evolution, Systematik und stratigraphische Bedeutung der neogenen Süßwassergastropoden von Rhodos und Kos/Ägäis. *Palaeontographica. Abt. A*, 174, 10-235.

Willmann, R. (1983) Neogen und jungtertiäre Entwicklung der Insel Kos (Agäis, Griechenland). *Geologische Rundschau*, 72(3), 815-860.

Yilmaz, Y., Genç, Ş.C., Gürer, F., Bozcu, M., Yilmaz, K., Karacik, Z., Altunkaynak, Ş, Elmas A. (2000) When Did the Western Anatolian Grabens Begin to Develop? In: Bozkurt, E., Winchester, J.A., Piper, J.D.A. (Eds.) *Tectonics and Magmatism in Turkey and the Surrounding Area*. Geological Society, London, Special Publications, 173, 353-384. https://doi.org/10.1144/GSL.SP.2000.173.01.17

Zachariasse W.J., van Hinsbergen D.J.J., Fortuin, A.R. (2011) Formation and fragmentation of a late Miocene supradetachment basin in central Crete: implications for exhumation mechanisms of high-pressure rocks in the Aegean forearc. *Basin Research*, 23(6), 678-701. https://doi.org/10.1111/j.1365-2117.2011.00507.x

Zahajská, P., Opfergelt, S., Fritz, S. C., Stadmark, J., Conley, D. J. (2020) What is diatomite? *Quaternary Research*, 96, 48–52. https://doi.org/10.1017/qua.2020.14

Zhang, G., Buatois, L. A., Mangano, M. G., Acenolaza, F. G. (1998) Sedimentary facies and environmental ichnology of a Permian playa-lake complex in western Argentina. *Paleogeography, Paleoclimatology, Paleoecology*, 138, 221-243. https://doi.org/10.1016/S0031-0182(97)00116-8

10. Figure captions

Figure 1: Simplified geological map (modified from Theodoropoulos, 1979) of Samos Island highlighting the Neogene sedimentary basins, with the location of the studied sections and correlatable observations. Sections are: 1) Pyrgos; 2) Paghondas; 3) Mavratzei; 4) Kavouraki; 5) Mytilini; 6) Stephania; 7) Antenna; 8) Hora; 9) Monasterio; 10) Pythagorion; 11) Marathokampos.

Figure 2: Stratigraphic columns showing the sedimentary infill of the Western Karlovassi and Eastern Mytilini basins, divided into five lithostratigraphic formations. Datum corresponds to the top of the Kokkarion Fm. The radiometric ages are from Weidmann et al. (1984) and Pe-Piper and Piper (2007). Abbreviations: B.Cg., Basal Conglomerate; OMB, Old Mill Beds; GB, Gravel Beds; WB, White Beds; MBB, Main Bone Beds; MT, Marker Tuffs.

Figure 3: Logs of measured stratigraphic sections of the Basal Conglomerate, Pythagorion and Hora formations (A) Mytilini Basin, (B) Karlovassi Basin. Location of the different sections in Figure 1. All correlations are based upon laterally continuous lithostratigraphic units (typically basalt flows or volcanic tuff), and remarkable surfaces. Datum corresponds to the top Hora – Base Mytilini Formations. Horizontal axis: Upper line: Ma, marls; M, Mudstone; W, Wackestone; P, Packstone; G, Grainstone; F/R, Floatstone/Rudstone; B, Boundstone. Lower line: C, Clay; S, Silt; VF, Very Fine-grained sandstone; F, Fine-grained sandstone; M, Medium-grained sandstone; C, Coarse-grained sandstone; Cg, Conglomerate.

Figure 4: Logs of measured stratigraphic sections of the Mytilini and Kokkarion formations (A) Mytilini Basin; (B) Karlovassi Basin. Location of the different sections in Figure 1. All correlations are based upon laterally continuous lithostratigraphic units (typically basalt flows or volcanic tuff), and remarkable surfaces. Datum corresponds to the top Hora – Base Mytilini Formations. Horizontal axis: Upper line: Ma, marls; M, Mudstone; W, Wackestone; P, Packstone; G, Grainstone; F/R, Floatstone/Rudstone; B, Boundstone. Lower line: C, Clay; S, Silt; VF, Very Fine-grained sandstone; F, Fine-grained sandstone; M, Medium-grained sandstone; C, Coarse-grained sandstone; Cg, Conglomerate.

Figure 5: Overview of the different terrigenous facies. Geologists, hammer, notebook and finger for scale. (A and B) Facies T1, normally graded, matrix-supported conglomerate. (C) Close-up view on facies T1, showing clasts of reworked carbonate facies in a silty/sandy matrix. (D) Facies T2, clast-supported, channelised (black lines), polygenic conglomerate. (E) Facies T2 with clast imbrication (black arrow) alternating with T3, a cross-bedded (white arrow), coarse to medium-grained sandstone. (F) Close-up view on facies T3, coarse to medium-grained sandstones with badly expressed planar lamination. (G) Facies T4, planar and lenticular beds of planar-laminated medium to fine-grained sandstones (black arrow) interbedded with facies T5, reddish silty claystones. (H) Facies T5, a reddish silty claystone with irregular and nodular pedogenetic levels (white arrow) alternating with volcanic tuff layers (Facies V1, black arrows). (I) Close-up view on facies T5, showing root traces.

Figure 6: Overview of the different volcaniclastic facies. Geologists, hammer, Jacob staff and pencil for scale. (A) Metre-scale alternation of facies V1 (subaerial volcanic tuff, grey layers) and Jacob staff facies T5. (B) Close-up view of facies V1, showing coarse, badly sorted materials. (C) Metres-thick layer of facies V2,

a yellowish tuff interbedded with facies C5. (D) Metre-scale turbiditic layer made of a greyish tuff (V2) interbedded with facies C9. (E) Close-up view at the base of this turbiditic layer, showing convoluted structures. (F) Microscopic (XPL) view of facies V2, made of subhedral to euhedral phenocrysts of plagioclase and pyroxene embedded in a matrix made of silt-size unidentified vitreous fragments.

Figure 7: Overview of the different carbonate facies (Part 1). Geologists, hammer and pencil for scale. (A) Facies C1, blue green marls, evolving toward the top in facies C2, a silty, gastropod mudstone to wackestone. (B) Whitish pedogenetic glaebules in facies C1. Pencil for scale. (C) Facies C2, silty, gastropod mudstone to wackestone with some preserved gastropods (back arrows). (D) Vertical thin root traces (black arrows) in facies C2. (E) Microscopic (PPL) view of facies C2, a wackestone with gastropod debris. (F) Microscopic (PPL) view of facies C3, a silty peloid packstone. Porosity in blue. (G) Metric tabular bed of facies C4, a silty peloid packstone with planar lamination. (H) Microscopic (PPL) view of facies C4, a peloid grainstone with ooids and gastropods debris. (I) Facies C5a, a well-stratified mudstone, forming tabular decimetre-thick beds. (J) Microscopic (PPL) view of facies C5a, showing a faint planar lamination. (K) Facies C5b, showing synsedimentary deformation and slump structure. (L) Facies C5b, with slumps, draped and overlain by planar conformable beds.

Figure 8: Overview of the different carbonate facies (Part 2). Geologists, hammer, finger and pencil for scale. (A) Close-up view of facies C6, a dolomudstone with leached gypsum cavities (black arrow) and facies C7, a laminated dolomudstone. (B) Microscopic (PPL) view of facies C6, showing leached gypsum cavities with rare remaining gypsum crystals. (C) Metre-thick alternation of facies C8, a whitish, well-stratified dolomudstone with greyish C6 and C7 facies. (D) Facies C9, characterised by the milimetre to centimetre-scale alternation of crinkled diatomite-rich laminae and carbonate laminae. (E) Microscopic (PPL) view of

facies C9, showing a recrystallised (silicified) diatomite-rich laminae, between two carbonate laminae. (F) Facies C10, an intraclastic and bioclastic wackestone to packstone. (G) Microscopic (PPL) view of facies C10, a packstone rich in charophyte gyrogonites and ostracod debris. (H) Microscopic (PPL) view of facies C10, a complex pore network formed by circum-granular cracks, and partially filled by a granular calcite (pink staining) cement (porosity in white). (I) Facies C12, a rudstone made of broken stem-moulds (phytoclasts). (J) Facies C11, a phytoherm framestone forming discontinuous patches and beds made of the amalgamation of stem moulds, in life position. (K) Microscopic (PPL) view of facies C11, showing the stem-mould structure made of alternating calcite micrite and spar to microspar laminae. (L) Facies C13, an oncoid (black arrows) and phytoclastic floatstone.

Figure 9: Synthesis and vertical distribution of the main palynological data (after Ioakim & Solounias, 1985; Ioakim et al., 2005; Ioakim & Koufos, 2009; Koufos et al., 2011), gastropods (after Koufos et al., 2011; Owen et al., 2011) and diatoms (Owen et al., 2011).

Figure 10: Results of oxygen ($\delta^{18}O$) and carbon ($\delta^{13}C$) stable isotope analyses (in ‰ relative to V-PDB) of the original micrite and dolomicrite, plotted vertically along four representative sections, divided by stratigraphic formations.

Figure 11: Results of oxygen ($\delta^{18}O$) and carbon ($\delta^{13}C$) stable isotope analyses (in ‰ relative to V-PDB) of the original micrite and dolomicrite, plotted in cross-plot diagrams for the different stratigraphic formations. The grey rectangle corresponds to calcite marine values. Correlation coefficient (r^2) are indicated and dashed lines correspond to trend line for covariant series. Location of the different sections in Figure 1.

Figure 12: Results of strontium isotope analyses ($^{87}Sr/^{86}Sr$ ratios) for the four representative sections, plotted stratigraphically and compared to the $^{87}Sr/^{86}Sr$ ratios from the Phanerozoic seawater curve (McArthur & Howarth, 2004). Stratigraphic positions of the different samples are approximate.

Figure 13: Depositional models for the Late Miocene succession from Samos Island. A) Basal Conglomerate and Pythagorion formations: brackish lake and wetland under wet climate; B) Hora Formation: deep salt lake model under dryer climate; C) Mytilini Formation: ephemeral alluvial system under dry conditions; D) Kokkarion Formation: palustrine and paludal tufa system under more humid conditions.

Figure 14: Structural models for the initiation and development of the Samos basins. See text for explanation.

Figure 15: (A) Geological time scale with global stages, mammal biozones and European land mammal ages, according to Hilgen et al. (2012). (B) Summary of the main palaeoenvironmental conditions in Samos (this study). (C) Summary of the main palaeoenvironmental conditions of the neighbouring regions of Samos Island. (D) Possible regional external forcing parameters.

Table 1: Summary of the main sedimentary facies identified in the iMiocene-Pliocene succession of the Samos basins and associated palaeoenvironmental interpretations.

Table S1: Stable isotope analyses (C, O, Sr) per sections and formations.

Lithofacies (Average thickness)	**Lithology/Texture**	**Bedding and sedimentary structures**	**Components**
(T1) Normally graded, matrix-supported conglomerate (1 – 3 m)	Matrix-supported polygenic breccia	- Irregular erosional base, erosional scours - Fining-upward, massive, badly stratified	- Basement clasts, cobble to pebble in size (marbles, quartz and schists) - Reddish coarse-grained sandstone matrix
(T2) Clast-supported, polygenic conglomerate (1 – 2 m)	Polygenic, clast-supported conglomerate	- Erosional basal surface - Clast imbrication, trough-cross bedding	- Basement clasts, cobble to pebble in size, Plant debris / Coarse-grained sandstone matrix

(T3) Coarse- to medium-grained sandstones with floating pebbles (10 cm – 1 m)	Coarse- to medium-grained, moderately sorted sandstone with floating pebbles	- Lower erosive surface and upper planar one. Fining-upward trend - Trough-cross bedding and plane parallel laminations	- Various material, depending of the area and formation: volcaniclastic material, quartz, carbonate lithoclasts
(T4) Planar-laminated medium- to fine-grained sandstones (10 – 50 cm)	Poorly sorted, medium- to fine-grained sandstone	- Discontinuous lenticular beds - Non-erosional, undulatory base - Planar horizontal lamination	- Reworked volcaniclastic material - Local granule lenses on bedding planes
(T5) Reddish silty claystone (10 cm – 1 m)	Mottled reddish to brownish, silty claystone	- Root traces, whitish nodules, desiccation cracks	- Silt-size subangular quartz grains - Some floating pebbles
(C1) Blue/green marls (10 cm – 2 m)	Silty marl	- Bioturbation, root traces and nodular carbonate concretions	- Gastropods, vegetal debris, pyrite
(C2) Silty, gastropod mudstone to wackestone rich in plant debris (10 cm – 1 m)	Marly mudstone to wackestone	- Bioturbation, root traces and nodular carbonate concretions - Fenestrae	- Gastropods, charophyte gyrogonites, vegetal debris - Silt-size quartz and clay
(C3) Silty peloid packstone (10 – 50 cm)	Well-sorted, silty peloid packstone	- Lower erosive surface	- Peloids, gastropod and ostracod debris, rare Characean gyronites. Clay clasts.
(C4) Peloid grainstone with ooids and gastropods (10 cm – 1 m)	Well-sorted grainstone	- Slightly erosive lower surface - Cross-bedding, Rare flat HCS-like	- Peloids, micritized ooids, intraclasts - A few gastropod debris and fish remain
(C5a & C5b) Well-stratified mudstone (5 – 10 cm)	White, sometime chalky, mudstone	- Non-erosional flat top and bottom surfaces, faint planar lamination - C5b: slumps, creeping balls, folds	- Micritic peloids, gastropods debris, intraclasts (less than 5 %) - Centimetre to decimetre-scale cherts
(C6) Dolomudstone with leached gypsum (10 – 20 cm)	Dark grey dolomudstone	- Planar irregular lamination - Dissolved gypsum lenses and nodules	Azoic
(C7) Laminated dolomudstone (10 – 20 cm)	Dark grey, planar-laminated bindstone	- Sub-horizontal, crinkly, laminae - Brecciation at top of beds. Fenestrae	Azoic
(C8) Well-stratified dolomudstne with cherts (10 – 20 cm)	Whitish, nearly azoic dolomudstone	Well-stratified tabular beds, with flat top and bottom surfaces	- Rare gastropods, rare, corroded diatoms - Dark-brown isolated chert nodules

(C9) Thinly laminated papyraceous diatomites (10 cm – 10's of m)	Mm- to cm-scale laminae of micrite, diatomite and diatomaceous silt	- Thinly laminated - Slumps, syn-sedimentary deformation - Broken laminae	Diatoms
(C10) Intraclastic limestone (10 cm – 1 m)	Greyish, poorly sorted, intraclastic and bioclastic wacke- to packstone	- Irregular base and top - Root moulds, circum-granular cracks - Pseudomicrokarstification	- Peloids, intraclasts, phytoclasts - Charophyte gyronites, gastropods, ostracods - Dark, silty micritic matrix00
(C11) Phytoherm framestone (20 cm – 1 m)	Beige, phytoherm framestone	Laterally discontinuous metric-scale patches and beds with irregular boundaries	- Amalgamation of mm- to cm-scale stem moulds, in life position, Charophyte gyronites, ostracods. Dark micritic to peloidal matrix.
(C12) Phytoclast rudstone (20 cm – 1 m)	Badly-sorted, phytoclast (silty) rudstone	Irregular bedding planes and root traces at their top	- Phytoclasts, gastropods, oncoids, charophyte thalli and gyrogonites. Dark, silty, micritic matrix
(C13) Oncoid and phytoclastic floatstone (20 cm – 1 m)	Oncoid and phytoclastic floastone	- Lower erosive surface and upper planar one. Fining-upward trend	- Gastropod debris, phytoclasts, intraclasts, oncoids. Dark beige silty micritic matrix
(V1) Subaerial volcanic tuffs (10 cm – 1 m)	Light grey volcanic tuff	- Laterally continuous, fining upward layers with sharp, but non erosive basal contact, and no internal truncation - Rare root traces	- Subhedral to euhedral phenocrysts of plagioclase and pyroxene - Matrix made of silt-size vitreous fragments
(V2) Subaqueous volcanic tuffs (10 – 50 cm)	Light grey volcanic tuff	- Massive layer, fining upward trend - Convolute, cross bedding, current ripples	- Subhedral to euhedral phenocrysts of plagioclase and pyroxene - Matrix made of silt-size vitreous fragments - Clasts of basalts and carbonates

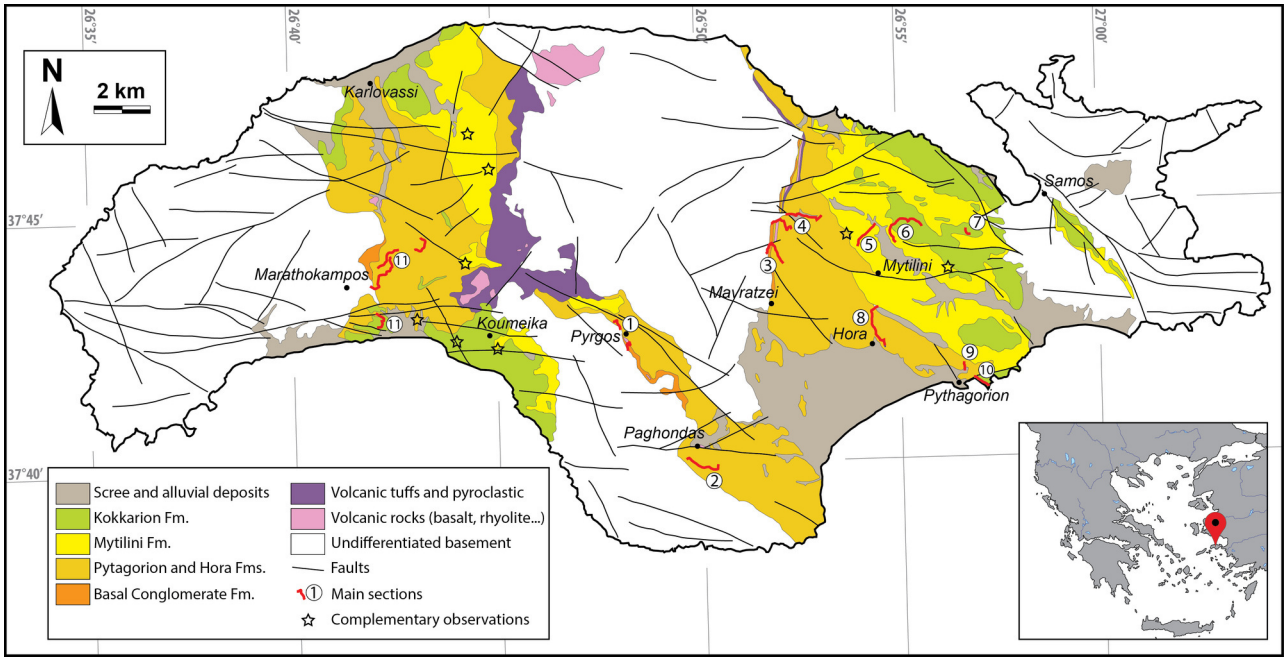

Figure 1 - location.jpg

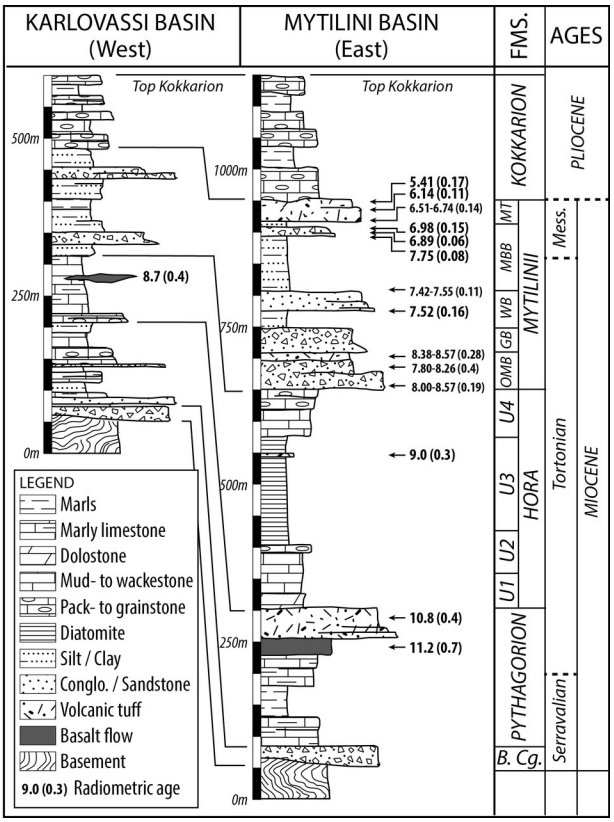

Figure 2 - strati.jpg

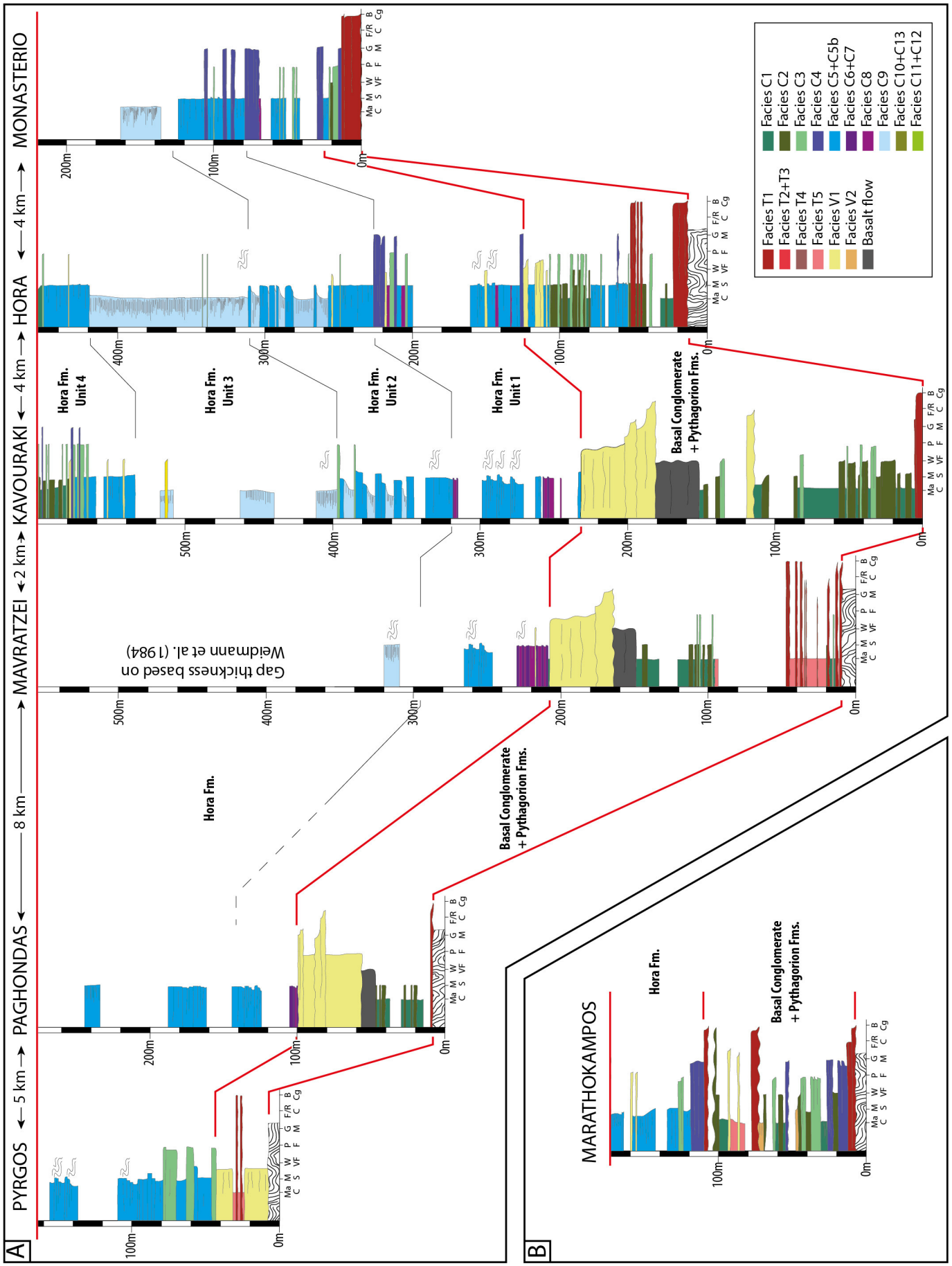

Figure 3 - logs Pytahgorion Hora.jpg

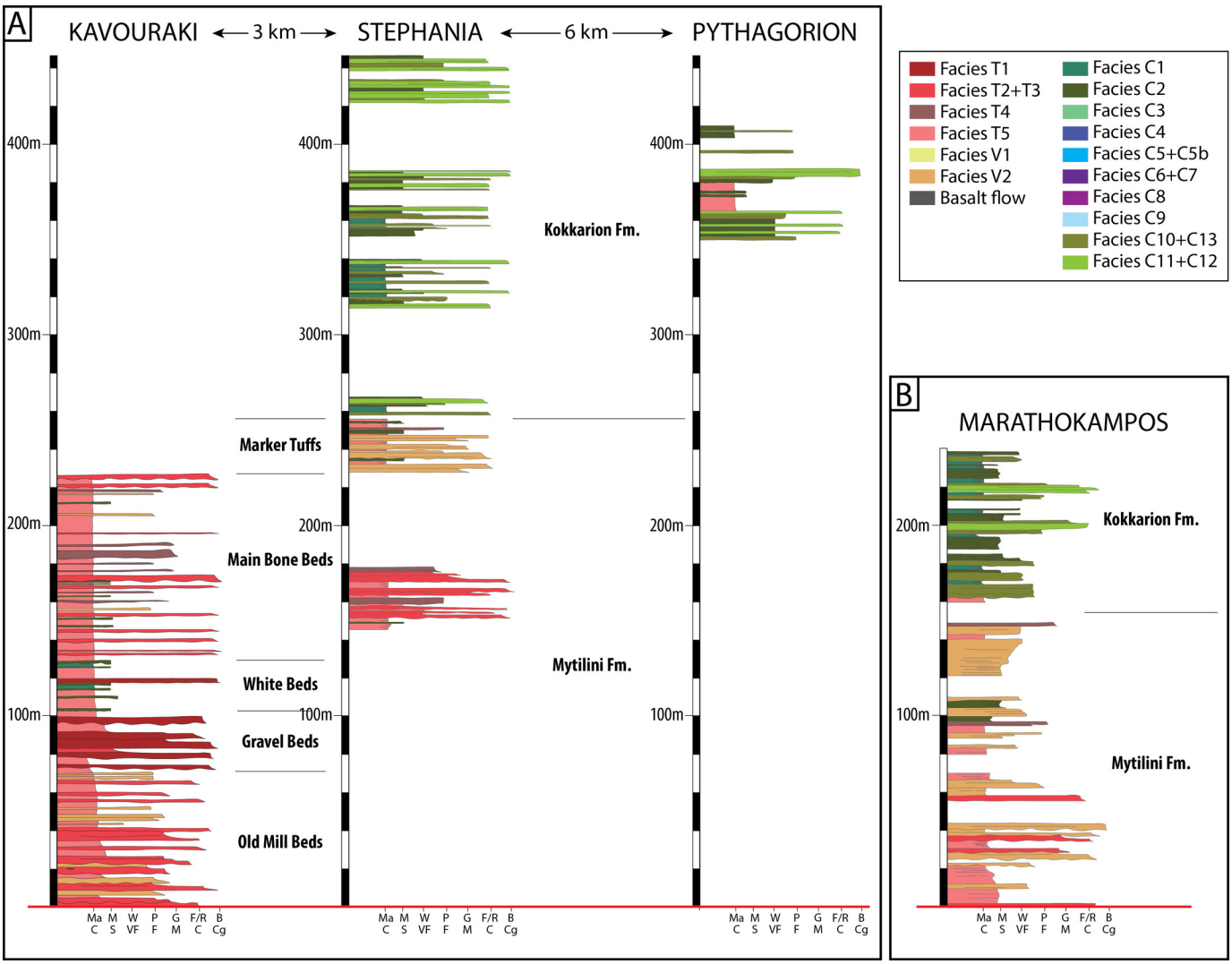

Figure 4 - logs Mytilini - Kokkarion.jpg

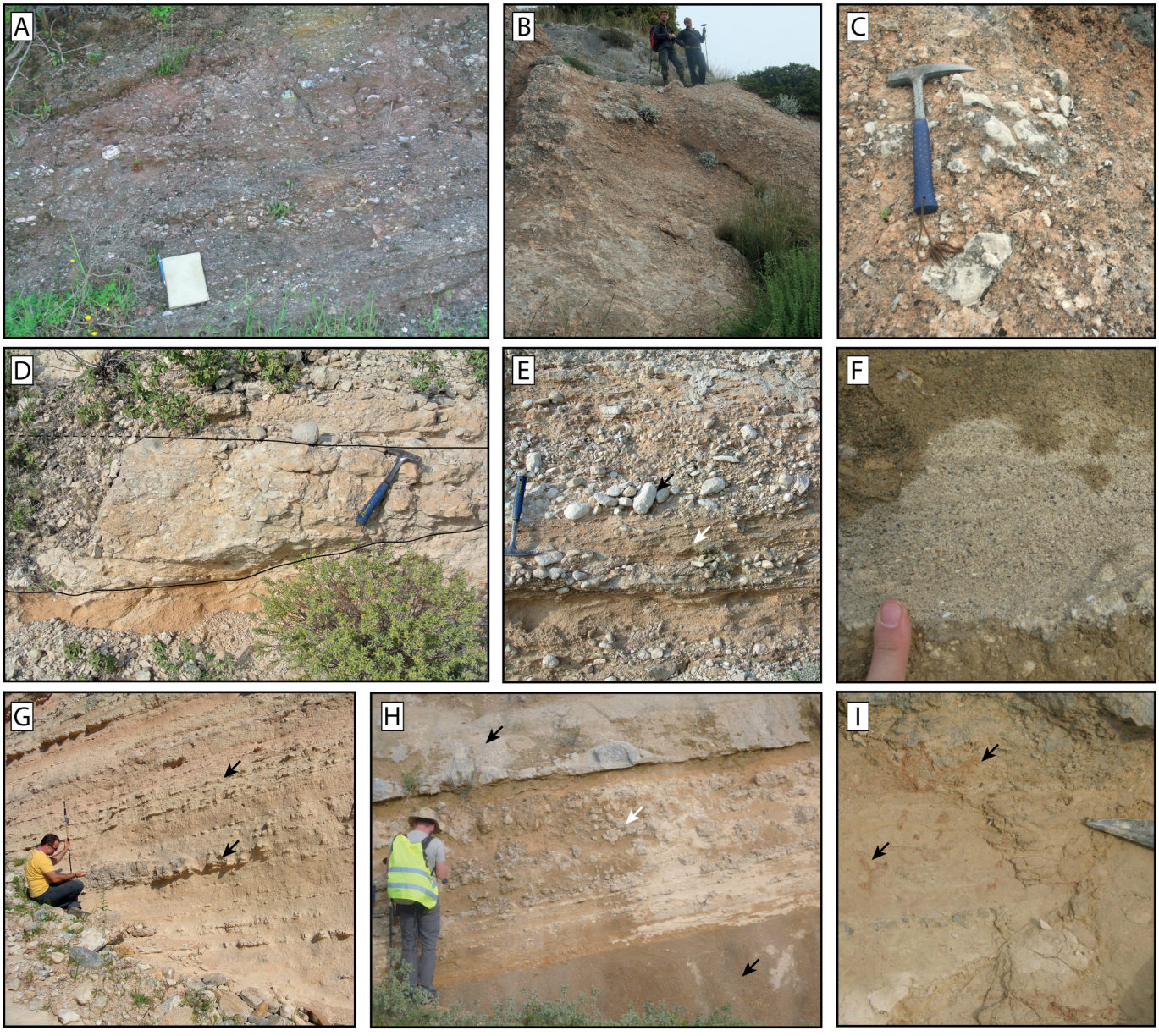

Figure 5 - Facies T.jpg

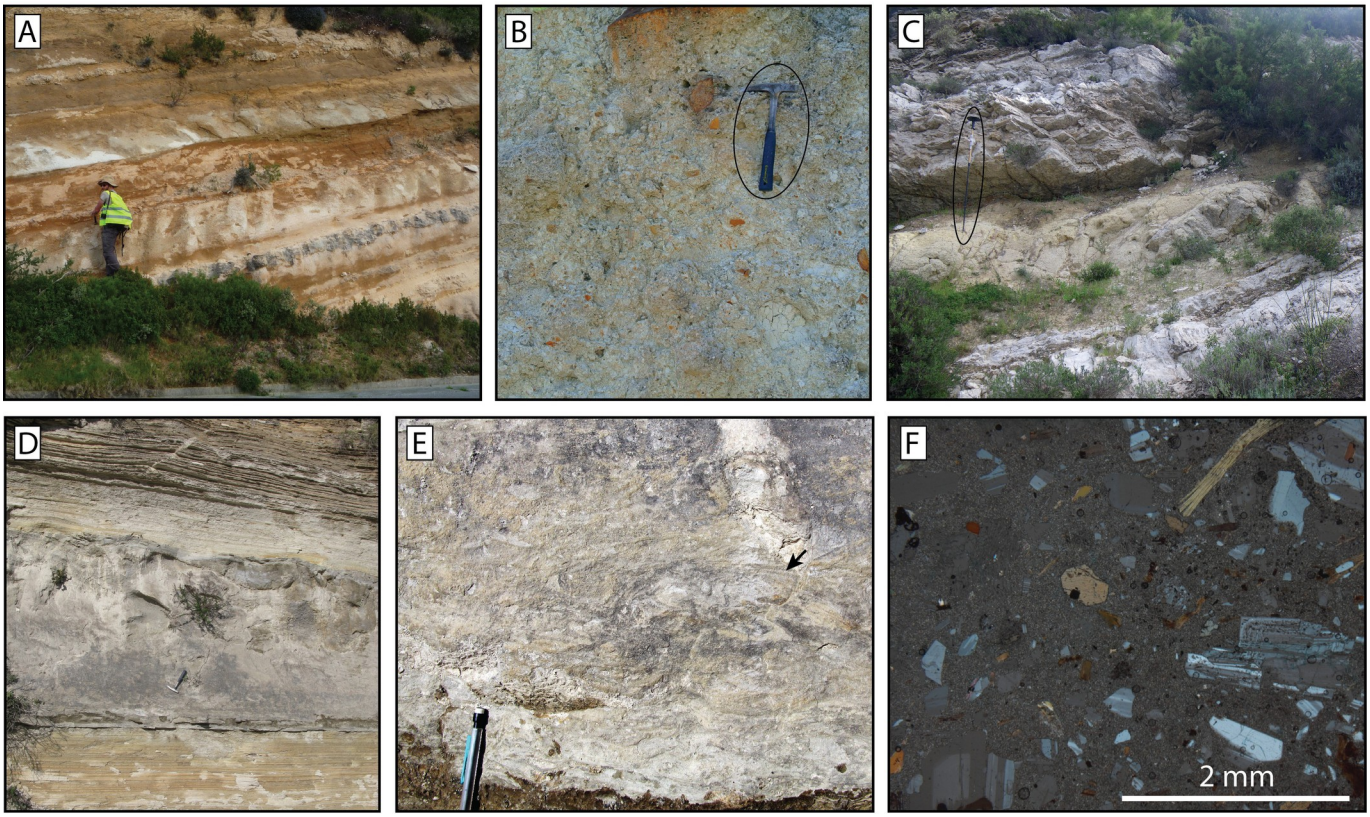

Figure 6 - Facies V.jpg

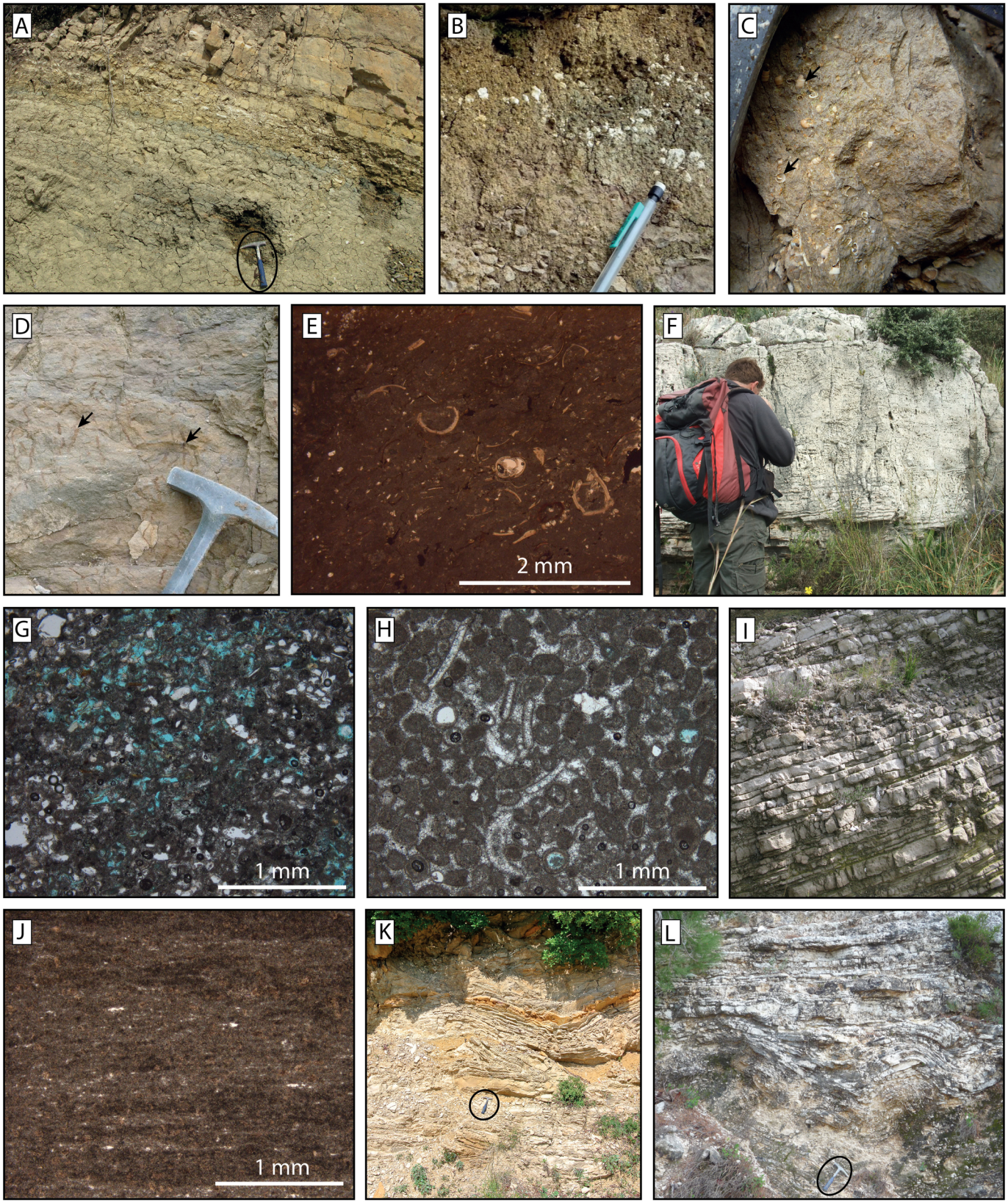

Figure 7 - Facies C1.jpg

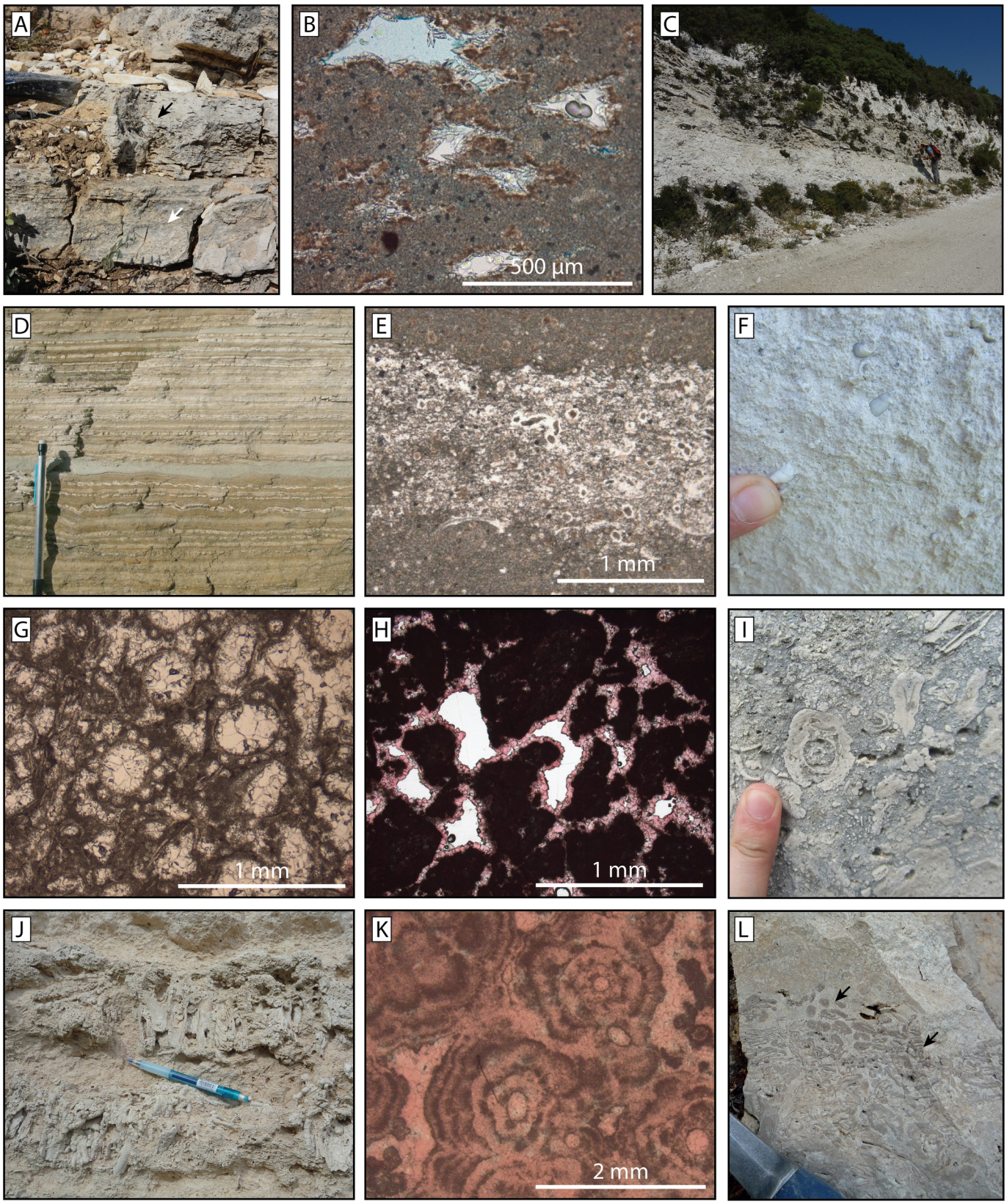

Figure 8 - Facies C2.jpg

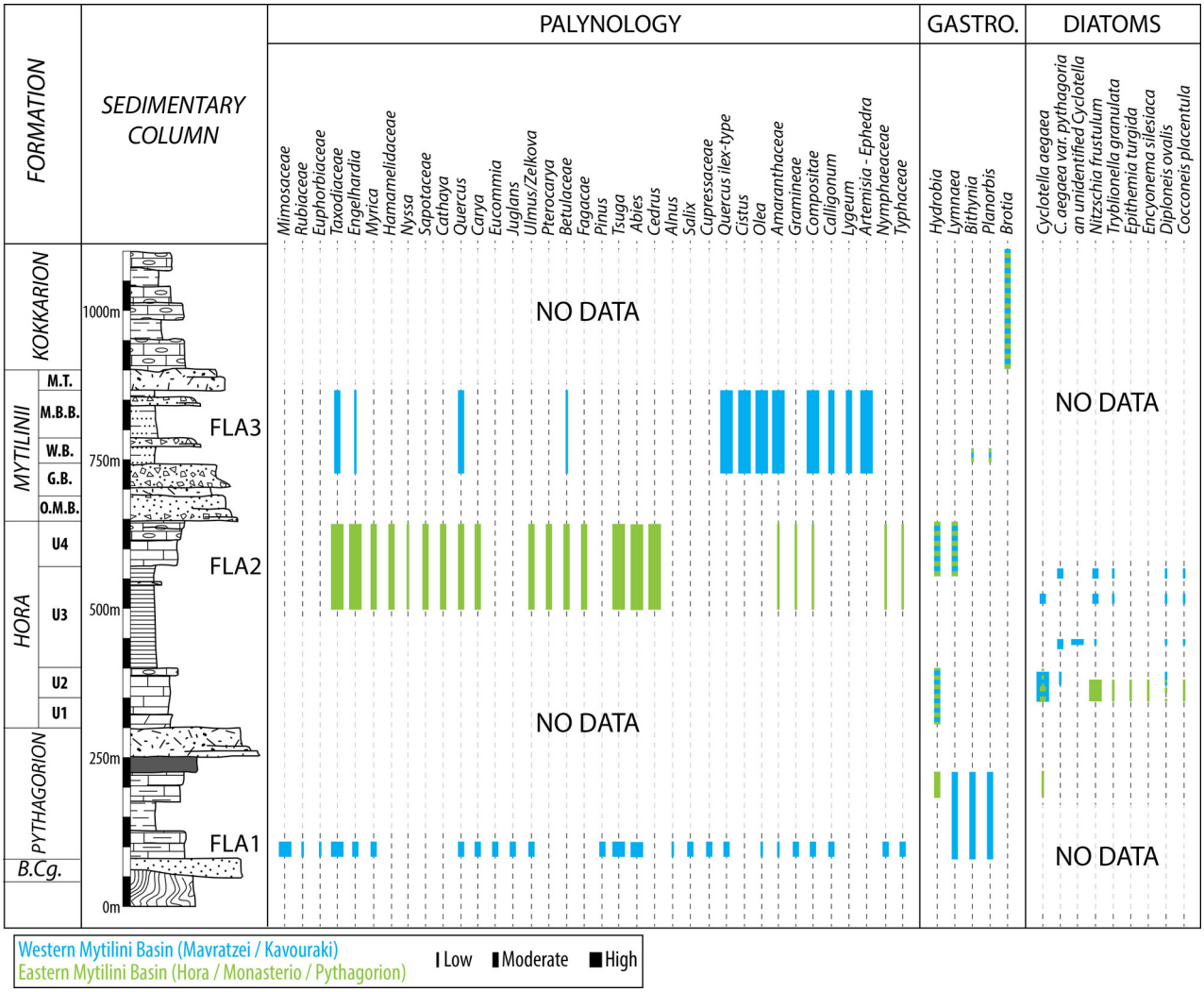

Figure 9 - Flora-Fauna.jpg

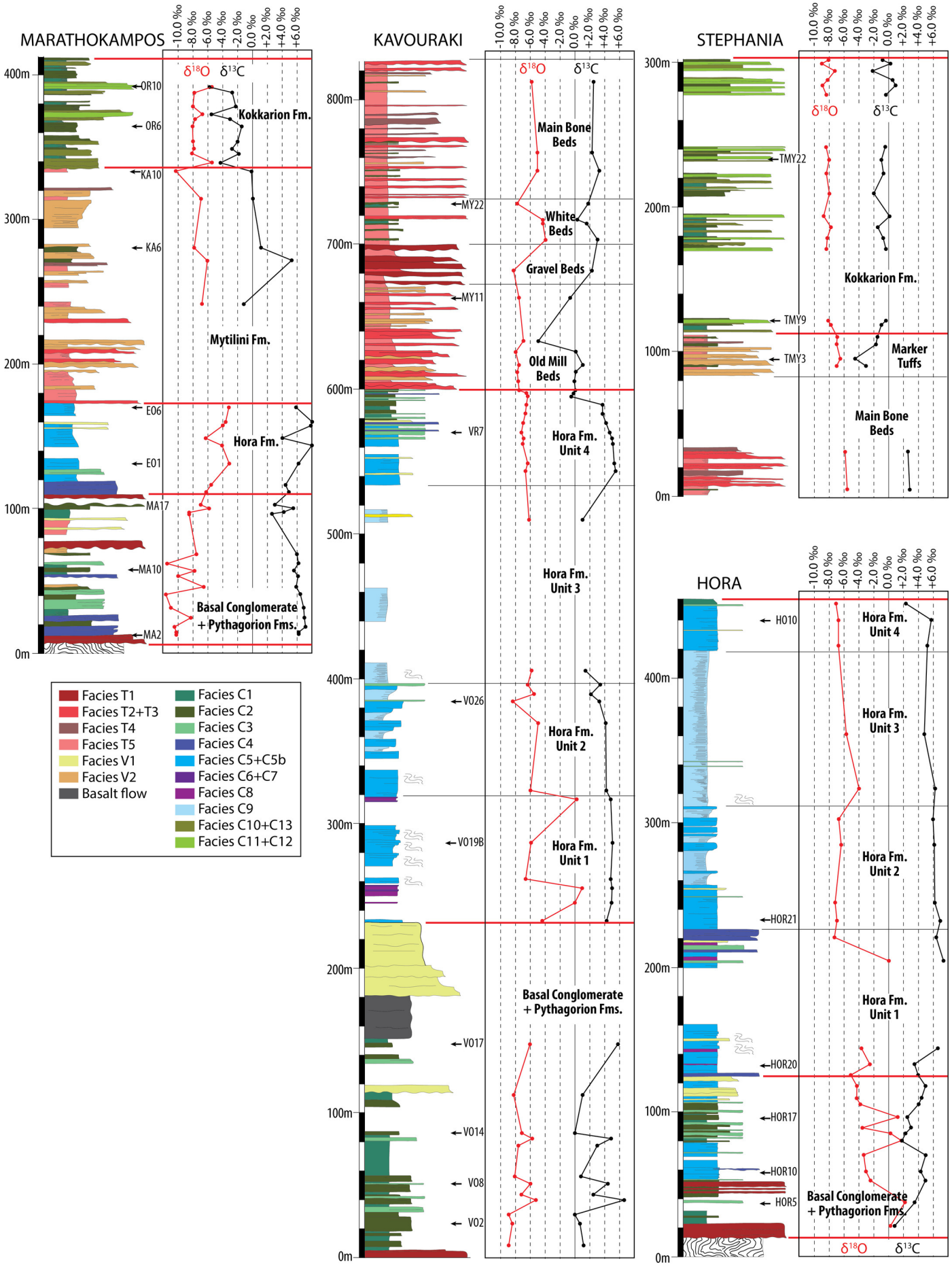

Figure 10 - C-O isotopes.jpg

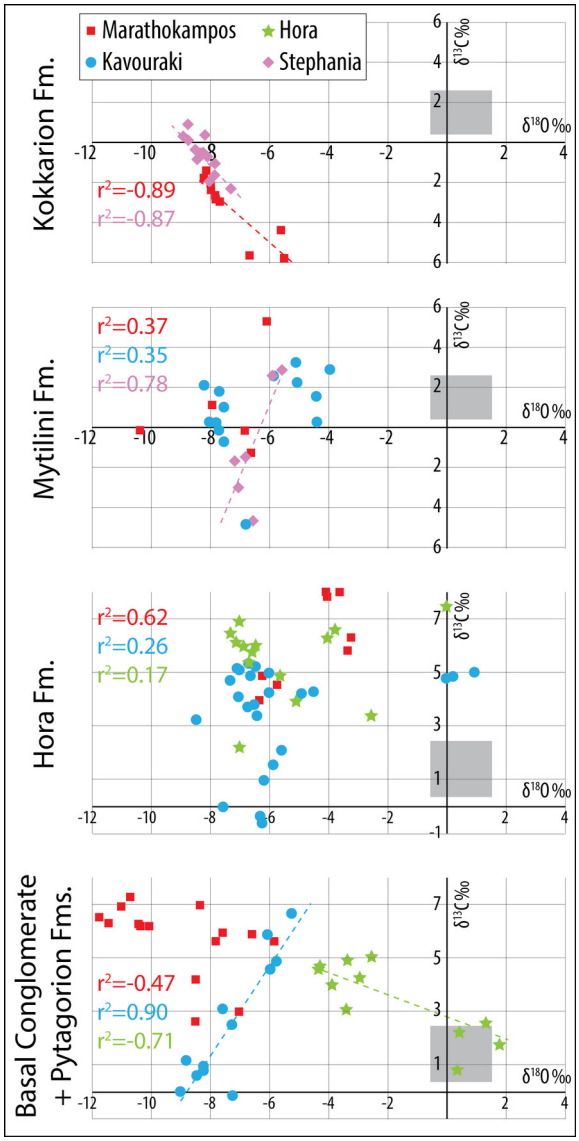

Figure 11 - C-O isotopes 2.jpg

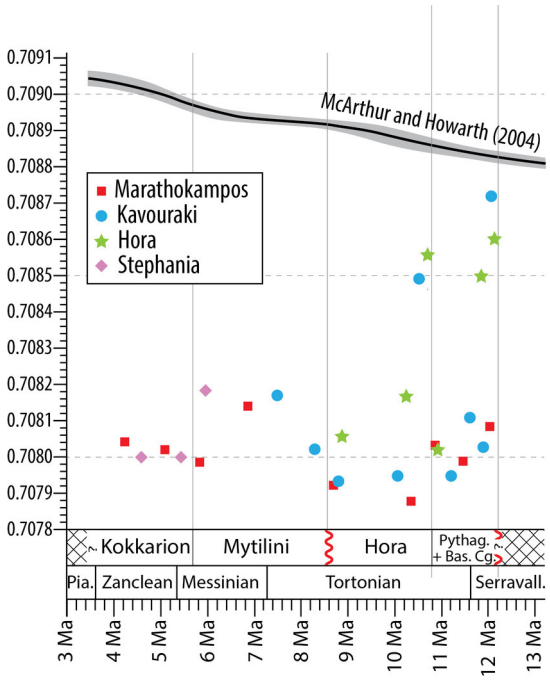

Figure 12 - Strontium.jpg

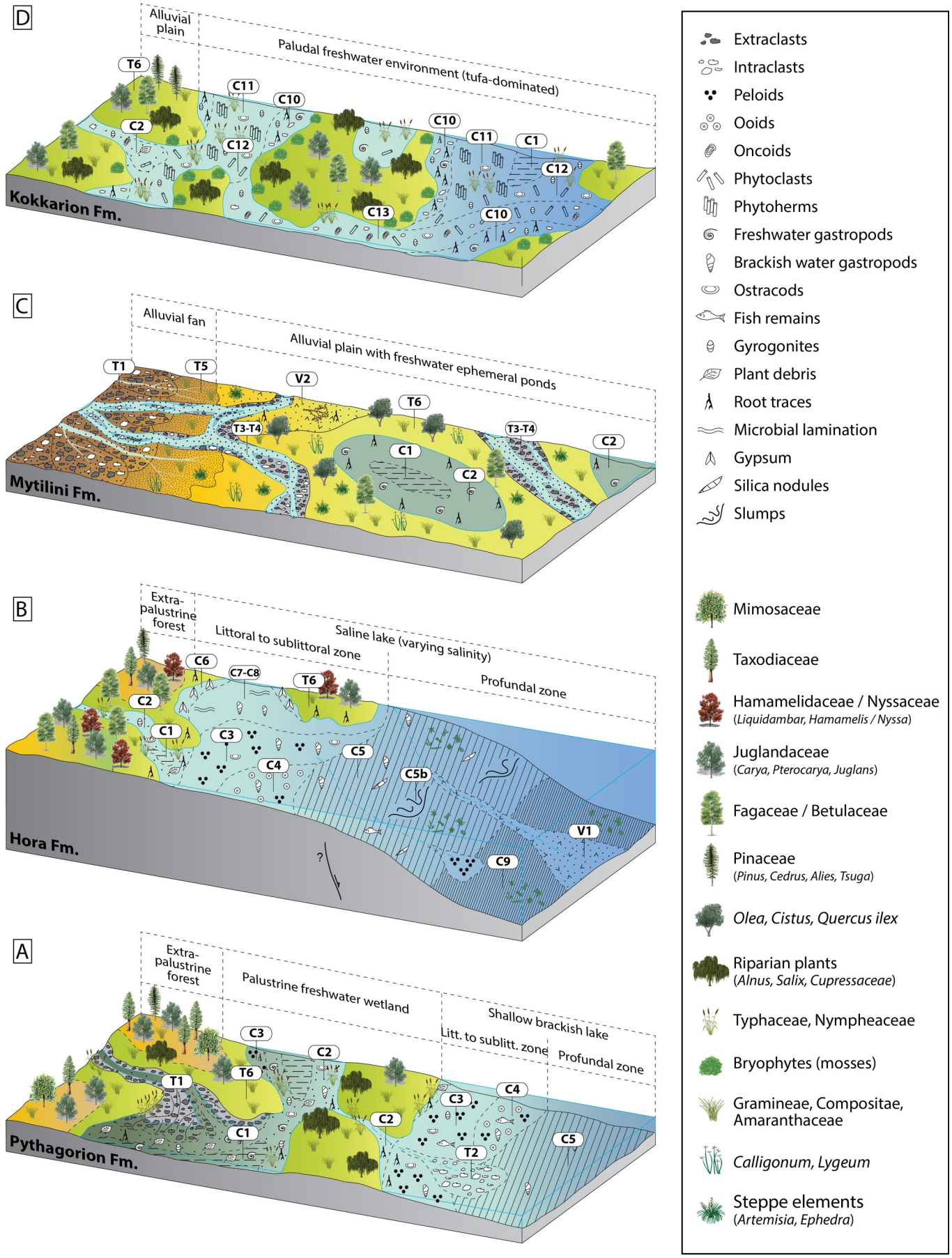

Figure 13 - Modeles Depots.jpg

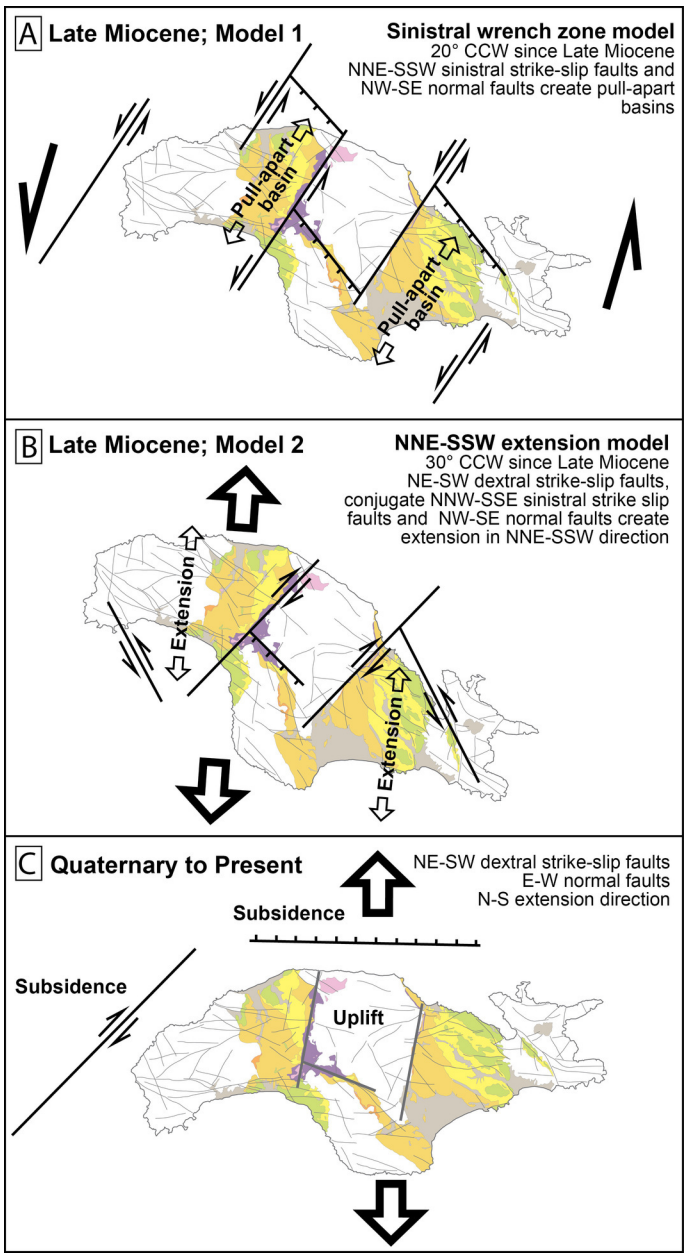

Figure 14 - Structurale.jpg

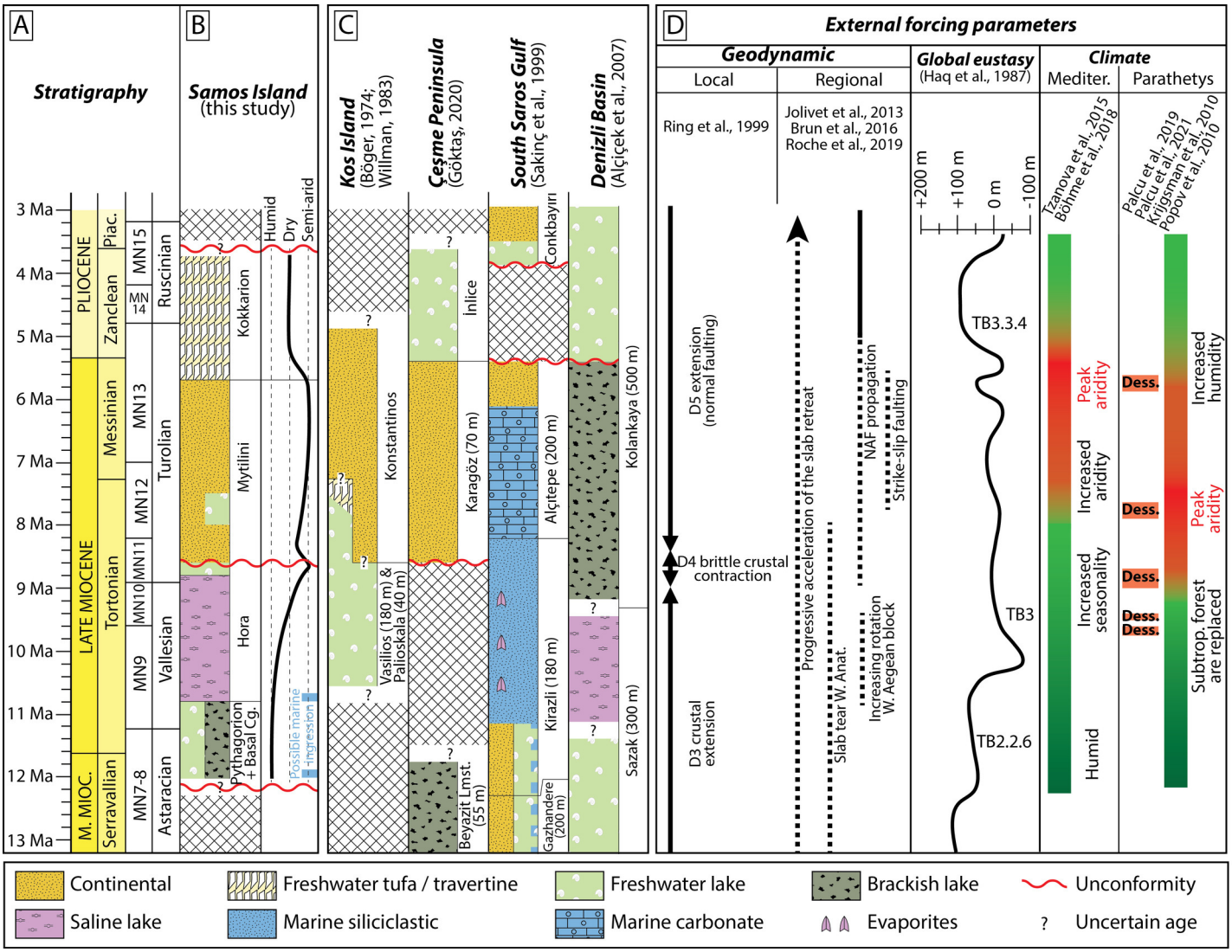

Figure 15 - Discussion regionale.jpg